

# Privacy Preserving Mechanisms for Coordinating Airspace Usage in Advanced Air Mobility

Chinmay Maheshwari\*, Maria G. Mendoza\*, Victoria Marie Tuck\*, Pan-Yang Su,  
Victor L Qin, Sanjit A. Seshia, Hamsa Balakrishnan, Shankar Sastry

## Abstract

Advanced Air Mobility (AAM) operations are expected to transform air transportation while challenging current air traffic management practices. By introducing a novel market-based mechanism, we address the problem of the on-demand allocation of capacity-constrained airspace to AAM vehicles with heterogeneous and private valuations. We model airspace and air infrastructure as a collection of contiguous regions (or sectors) with constraints on the number of vehicles that simultaneously enter, stay, or exit each region. Vehicles request access to the airspace with trajectories spanning multiple regions at different points in time. We use the graph structure of our airspace model to formulate the allocation problem as a path allocation problem on a time-extended graph. To ensure that the cost information of AAM vehicles remains private, we introduce a novel mechanism that allocates each vehicle a budget of “air-credits” (an artificial currency) and anonymously charges prices for traversing the edges of the time-extended graph. We seek to compute a competitive equilibrium that ensures that: (i) capacity constraints are satisfied, (ii) a strictly positive resource price implies that the sector capacity is fully utilized, and (iii) the allocation is integral and optimal for each AAM vehicle given current prices, without requiring access to individual vehicle utilities. However, a competitive equilibrium with integral allocations may not always exist. We provide sufficient conditions for the existence and computation of a fractional-competitive equilibrium, where allocations can be fractional. Building on these theoretical insights, we propose a distributed, iterative, two-step algorithm that: 1) computes a fractional competitive equilibrium, and 2) derives an integral allocation from this equilibrium. We validate the effectiveness of our approach in allocating trajectories for two emerging urban air mobility services: drone delivery and air taxis.

**Key Words and Phrases:** Advanced Air Mobility, Competitive Equilibrium, Distributed Algorithm, Artificial Currency

---

\*Chinmay Maheshwari, Maria G. Mendoza, and Victoria Tuck contributed equally to this work and are listed alphabetically.

Authors’ Contact Information: Chinmay Maheshwari, Maria G. Mendoza, Victoria Tuck, Pan-Yang Su: {chinmay\_maheshwari, maria\_mendoza, victoria\_tuck, pan\_yang\_su}@berkeley.edu, University of California, Berkeley; Victor L Qin, victorqi@mit.edu, MIT School of Engineering; Sanjit A. Seshia, seshia@eecs.berkeley.edu, University of California, Berkeley; Hamsa Balakrishnan, hamsa@mit.edu, MIT School of Engineering; Shankar Sastry, sastry@coe.berkeley.edu, University of California, Berkeley.

# 1 Introduction

The emergence of advanced air mobility (AAM) operations, including urban air mobility (UAM) and unmanned aerial vehicles (UAVs), is expected to transform the landscape of the air transportation system. These new aerial platforms can provide air taxi services that better connect rural and suburban communities with urban centers, facilitate package and medical delivery services, and support infrastructure and public safety (Guo et al., 2024). However, these new technologies bring new challenges concerning air traffic management. Current estimates of the density, type, and number of these new flights have led the Federal Aviation Administration (FAA) in the United States to declare that “existing Air Traffic Management (ATM) system infrastructure and associated resources cannot cost-effectively scale to deliver services” (Administration, 2022). While current systems focus primarily on fixed-wing aircraft, scheduled flight operations, and airport infrastructure, AAM includes novel electric vertical take-off and landing (eVTOL) aircraft and UAVs that will fly on demand, which creates challenges for scheduling flights. Additionally, like current aerial operations (Ball et al., 2018, 2020), AAM operations will have heterogeneous valuations for timely airspace access (while a passenger air taxi may be traveling on a strict schedule, a regional cargo flight could be delayed with less issue (Seuken et al., 2022; Skorup, 2019)), yet it is extremely important for these valuations to remain private because they can contain important business or personal information. These characteristics have led the FAA and other aviation agencies to call for novel air traffic management tools and strategies, developed by third-party Service Providers (SPs), to support AAM aircraft and use cases. These tools must work in conjunction with existing Air Navigation Service Providers (ANSPs, e.g., the FAA) to safely and efficiently actualize new air transport opportunities (Administration, 2022; European Organisation for the Safety of Air Navigation (EUROCONTROL), 2022; Federal Aviation Administration, 2023).

We propose an algorithm that schedules AAM vehicles with heterogeneous, private valuations requesting access to airspace in an on-demand manner. While ideas from conventional air traffic management (Bertsimas and Patterson, 1998, 2000; Bertsimas et al., 2011; Odoni, 1987; Roy and Tomlin, 2007) can accommodate private and heterogeneous valuations from flight operators, they are not designed for the dynamic and adaptable nature of AAM operations (Seuken et al., 2022; Skorup, 2019). This work aims to answer the following question:

Can we design an efficient mechanism that allocates desired airspace resources to AAM vehicles with heterogeneous private valuations without requiring them to disclose their valuations to anyone?

To address this, we model the airspace as a set of contiguous regions, each with specific capacity constraints on the number of AAM vehicles (modeled as eVTOLs) that can arrive, depart, or stay at any given time (see Fig. 1). Vehicles submit requests for airspace access through a menu of time-trajectories (or air corridors), detailing which regions they will occupy at different time steps. We frame the allocation of these time-trajectories within capacity-constrained airspace as a path allocation problem on a time-extended graph (Definition 2.1), where all capacity constraints are represented as constraints on the graph’s edges.

We introduce a new mechanism with artificial currency that is implemented in a receding horizon manner. In every round of this approach, the SP allocates “air-credits” (the artificial currency) to each AAM vehicle requesting access to airspace in that round and charges an anonymous price (in air credits) for the use of various airspace regions. Based on these prices, each vehicle calculates its most preferred bundle of regions

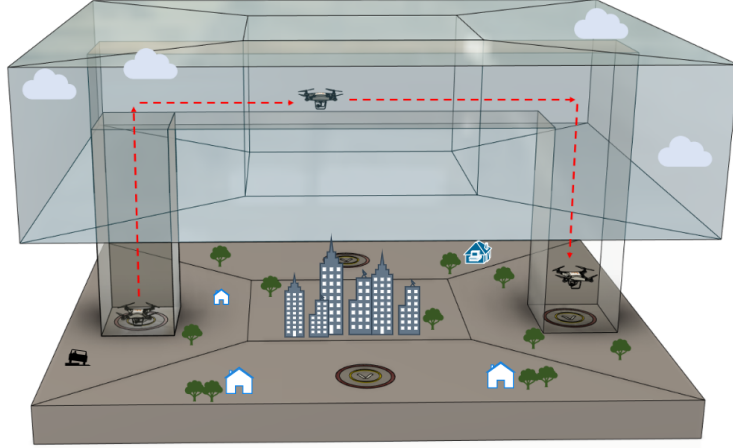


Figure 1: Model of airspace as a set of contiguous regions, each having arrival, departure, and transit constraints. Some regions are at the cruising altitude, while others encompass vertiport/launch pads.

on the time-extended graph that maximizes its valuation while adhering to its budget constraint and some additional *individual constraints* to ensure that the set of bundles forms a feasible path.

The goal of the SP is to design prices and allocate airspace regions efficiently and safely, guided by the following desiderata: *(i)* Given the price vector, the allocation by the SP should be optimal for every AAM vehicle, maximizing each vehicle’s private valuation subject to budget constraints; *(ii)* The capacity constraints of the airspace must be respected; *(iii)* Prices must be non-negative, and if they are strictly positive, the capacity of each airspace region must equal its demand. A tuple of allocation and prices that satisfy these requirements is referred to as a *competitive equilibrium* in economics, which may not always exist (Budish, 2011). However, inspired by the literature on Fisher markets under linear constraints (Jalota et al., 2023), we demonstrate that a *fractional competitive equilibrium* — a relaxation of the competitive equilibrium that allows fractional allocations — always exists (Proposition 3.3). Furthermore, we show that the prices at a fractional-competitive equilibrium can be computed as an optimal dual multiplier of a “budget-adjusted welfare problem” (see (3)), which is a convex optimization problem (Lemma 3.4). Notably, the budget adjustment for each vehicle is determined by the optimal dual multiplier associated with its individual constraints. As a result, computing a fractional-competitive equilibrium reduces to calculating a fixed point (Proposition 3.5).

Building on these theoretical insights, we propose a *two-step algorithmic procedure* to allocate AAM vehicles to airspace. In the first step, we develop a *two-loop* algorithm to compute the fractional-competitive equilibrium without requiring information about the private valuations of vehicles. Specifically, this step involves solving the fixed point problem stated in Proposition 3.5 via a two-loop algorithm (see Algorithm 1) that mimics fixed point iteration. The inner loop solves a reformulated budget-adjusted welfare problem in a distributed manner using an Alternating Direction Method of Multipliers (ADMM) update, ensuring that AAM vehicles do not have to share their valuations with anyone. The outer loop then updates the budget adjustment parameter using the most recent value of the dual multiplier corresponding to the individual constraints of the AAM vehicles.

In the second step, we derive an integral allocation from the fractional-competitive equilibrium obtained

in the first step, keeping the prices unchanged. We rank the vehicles based on the fractional allocation they received for their most desired resource in the first step. The social planner then allocates resources to the vehicles sequentially according to this ranking, updating the remaining capacity after each allocation (Algorithm 2).

Algorithm 1 can be viewed as feedback between the learning algorithm used by AAM vehicles and the SP. The AAM vehicles use (anonymized) signals from the SP, such as prices and other parameters, to adjust their demand for resources. The SP, in turn, uses the updated demand for resources from each AAM vehicle to adjust the prices and related variables. Notably, this two-step process (Algorithms 1-2) does not require vehicles to disclose their private valuations to either the SP or to other vehicles (Remark 4.2). To validate the effectiveness of our approach, we explore two upcoming applications. First, we analyze drone-based package delivery using a dataset of drone trajectories generated with realistic physical models by Airbus over the city of Toulouse, France. Second, we investigate the scheduling problem for electric air taxis on a hypothesized air traffic network in Northern California, United States.

## 1.1 Related Works

**Market mechanisms for airspace management.** Su et al. (Su et al., 2024) utilized a generalized Vickrey–Clarke–Groves (VCG) auction for AAM resource management taking into account social welfare, safety, and congestion while considering proportional fairness by weighting different fleet operators accordingly. We adopt a similar time-extended graph model from their work to represent airspace with capacity constraints. However, when agents have budget constraints, as in our case, truthful bidding is no longer a dominant strategy (Ausubel and Milgrom, 2004), which limits the applicability of VCG-based mechanisms. Furthermore, the requirement for truthful bidding poses privacy concerns for vehicles as they have to reveal their exact valuations through bids. Other proposed approaches include second-price auctions combined with congestion management algorithms (Chin et al., 2023; Qin and Balakrishnan, 2022) and combinatorial auctions (Leet and Morris). Unlike our approach, these related works only considered unit-capacity regions.

Balakrishnan and Chandran’s work (Balakrishnan and Chandran, 2017) introduced a column generation algorithm that dynamically updates prices to respect capacity constraints, approximating a competitive equilibrium. Their approach, however, requires aircraft to report both their desired trajectory and the associated benefits. In contrast, our ADMM-based approach simplifies the process by requiring aircraft to report only their desired trajectories in response to announced prices. While the former approach may benefit from computational efficiency due to the additional information available to the central planner, our approach prioritizes privacy by limiting the amount of information shared. Another key distinguishing feature of our work, compared to existing market mechanisms for AAM, is the use of artificial currency. While, as noted by (Seuken et al., 2022), money can effectively elicit preferences, mechanisms involving monetary transactions may disproportionately favor operators with greater financial resources. Our approach mitigates this issue by introducing a system of artificial currency that helps ensure fairness.

**Connections with other economic mechanisms.** Our airspace allocation formulation incorporates four essential features: complementarities, indivisibilities, the absence of monetary transfers, and quasilinear preferences. In settings with substitutable and divisible goods, the classical concept of Competitive Equilibrium from Equal Incomes (CEEI) ensures efficient and fair outcomes by endowing agents with

an artificial currency that holds no value outside the market (Varian, 1974). However, in cases involving complementary and indivisible goods, a competitive equilibrium may not exist. A common approach in such cases is to seek an approximate CEEI (A-CEEI), which preserves efficiency, fairness, and incentive properties while being supported by computationally efficient algorithms tested in real-world applications like course allocation (Budish, 2011; Budish et al., 2023).

Although we adopt the idea of artificial currency, we deviate from this model by allowing agents to save currency for future use. When the saved budget influences the agent’s utility in a quasilinear form, our model more closely aligns with combinatorial auction environments, where monetary transfers play a role in eliciting agents’ preferences.

Combinatorial auctions allow participants to bid on combinations of items rather than individual items (Cramton et al., 2006a). Given the inherent exponential complexity of these auctions, there is no universal format that applies in all settings. Below, we highlight formats particularly suited to scenarios with budget constraints and strong complementarities. For a more comprehensive list, refer to (Cramton et al., 2006b, Table 2.2). In environments with budget constraints, dynamic auction formats often outperform static mechanisms like VCG auctions. These formats allow agents to observe current prices and adjust their bids according to their budget constraints before final submission. Examples include the Simultaneous Ascending Auction, the Ascending Proxy Auction, and the Clock-Proxy Auction (Ausubel and Cramton, 2004; Cramton et al., 2006b). These dynamic formats have an additional advantage: bids are submitted incrementally, reducing the risk of privacy violations and preventing the exponential growth of bundle combinations. However, they are still susceptible to computational complexity issues, which can even be exacerbated due to the inherent nature of combinatorial auctions. In our approach, we model complementarities using linear equality constraints and leverage recent advances in Fisher markets with linear constraints to develop an algorithmic approach that only needs to solve convex optimization problems.

Particularly, we compute a fractional-competitive equilibrium, which provides a relaxed solution that is easier to compute. From this fractional-competitive equilibrium, we then derive an integral allocation that satisfies the capacity constraints in the problem.

## 1.2 Organization

The article is organized as follows: In Section 2, we introduce the model of airspace management studied in this paper. In Section 3, we describe the proposed market mechanism with artificial currency and the theoretical results on fractional-competitive equilibrium. Section 4 presents the algorithmic procedure to compute an approximate market mechanism. In Section 5, we validate the performance of our mechanism using a drone delivery dataset generated based on a real drone dynamics model from Airbus. In Section 6, we study an additional AAM scenario of vertiport reservation for air-taxi services in Northern California. We conclude this study in Section 7 and state some interesting directions for future work. Proofs and additional supplementary material are provided in the appendix. In Section A, we present a simple example to illustrate the time-extended graph and constraints (2b)-(2c). In Section B, we provide proofs for all theoretical results discussed in this paper. Finally, in Section C, we consolidate all important notations used in this work in the form of a table.

## 2 Model of Advanced Air Mobility

Consider the problem of scheduling Advanced Air Mobility (AAM) vehicles, such as drones and eVTOLs, while facilitating novel AAM services in urban airspace. In our model, we segment the urban airspace into contiguous regions or sectors. We denote the set of regions as  $\mathcal{R}$ . The spatial layout of the airspace is represented as a graph  $\mathcal{G} = (\mathcal{R}, \mathcal{E})$ , where  $\mathcal{R}$  corresponds to the set of vertices of graph  $\mathcal{G}$ , and  $\mathcal{E} \subseteq \mathcal{R} \times \mathcal{R}$  represents the set of edges that connect contiguous regions, indicating the feasible movement of AAM vehicles. We model AAM vehicles arriving dynamically throughout the day, dividing the entire day into  $T$  time intervals (for example, 1-minute intervals). The set of AAM vehicle requests arriving in the system<sup>1</sup> at time  $t$  is denoted by  $U(t)$ . Every AAM vehicle  $u \in U(t)$  has a desired “menu” of time-trajectories, also known as “air-corridors,” one of which it prefers to follow in the airspace. We denote the requested menu for the AAM vehicle  $u \in U(t)$  as  $M_u$ <sup>2</sup> (to be defined formally later). Due to capacity constraints, it may not be feasible to allocate the most preferred time-trajectory to all AAM vehicles, as doing so might violate airspace constraints. Specifically, each region has a limit on the number of vehicles that can simultaneously arrive, depart, and stay in that region at any given time<sup>3</sup>. We denote  $C^{arr}(r, t)$ ,  $C^{dep}(r, t)$  and  $C^{stay}(r, t)$  to be the number of vehicles that can arrive, depart and stay in region  $r \in \mathcal{R}$  at any instance of time  $t$ , respectively<sup>4</sup>.

A service provider (SP) is responsible for managing the airspace and allocating each AAM vehicle a feasible time-trajectory from its menu while ensuring compliance with airspace constraints. To facilitate this process, we introduce the framework of a *time-extended graph*, which is essential for integrating arrival, departure, and transit constraints when allocating time-trajectories to AAM vehicles.

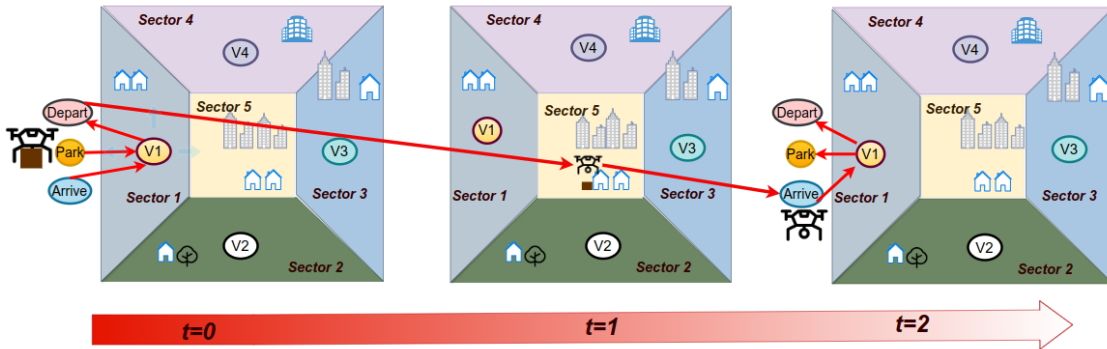


Figure 2: A time-trajectory of a drone delivering a package in an urban setting. The drone starts from the launch pad V1 (Sector 1) and needs to drop a package in Sector 5 before returning. Here, we have shown a simple trajectory that moves between regions in one time step, but in general, such trajectories can remain in any region for multiple rounds.

**Definition 2.1** (Time-extended Graph). We define  $\tilde{\mathcal{G}} = (\tilde{\mathcal{R}}, \tilde{\mathcal{E}})$  as the time-extended graph with horizon  $T$ , for some positive integer  $T$ , such that

<sup>1</sup>We assume that  $T$  is sufficiently large to allow us to round the arrival time of each AAM vehicle to the beginning of the corresponding time interval.

<sup>2</sup>The set  $M_u$  includes an option for the vehicle to drop out of the system, denoted by  $\emptyset$ .

<sup>3</sup>This constraint arises from safety concerns that limit the number of vehicles that can be autonomously deconflicted in a confined space (Bauranov and Rakas, 2021).

<sup>4</sup>The arrival and departure constraints are primarily required for airspace regions comprising of vertiports/launch-pads.

(i)  $\tilde{\mathcal{R}} = \cup_{t=1}^T \cup_{r \in \mathcal{R}} \{\nu(r, t), \nu^{arr}(r, t), \nu^{dep}(r, t)\}$ , where  $\nu(r, t)$ ,  $\nu^{arr}(r, t)$ , and  $\nu^{dep}(r, t)$  are three replicas of region  $r$  at time  $t$ .

(ii)  $\tilde{\mathcal{E}} = \cup_{j=1}^4 \tilde{\mathcal{E}}^{(j)} \subseteq \tilde{\mathcal{R}} \times \tilde{\mathcal{R}}$ , where

- $\tilde{\mathcal{E}}^{(1)} := \cup_{t=1}^T \{(\nu^{arr}(r, t), \nu(r, t))\}$ . Any edge of the type  $(\nu^{arr}(r, t), \nu(r, t))$  has capacity  $C^{arr}(r, t)$ .
- $\tilde{\mathcal{E}}^{(2)} := \cup_{t=1}^T \{(\nu(r, t), \nu^{dep}(r, t))\}$ . Any edge of the type  $(\nu(r, t), \nu^{dep}(r, t))$  has capacity  $C^{dep}(r, t)$ .
- $\tilde{\mathcal{E}}^{(3)} := \cup_{t=1}^{T-1} \{(\nu(r, t), \nu(r, t+1))\}$ . Any edge of the type  $(\nu(r, t), \nu(r, t+1))$  has the capacity of  $C^{stay}(r, t)$ .
- $\tilde{\mathcal{E}}^{(4)} := \cup_{t=1}^{T-1} \cup_{(r, r') \in \mathcal{E}} \{(\nu^{dep}(r, t), \nu^{arr}(r', t+1))\}$ . Any edge of the type  $(\nu^{dep}(r, t), \nu^{arr}(r', t+1))$  is unconstrained.

A simple example describing the time-extended graph is provided in Section A.

The menu for any AAM vehicle  $u \in U(t)$  is defined as  $M_u = R_u \cup \{\emptyset\}$ , where  $R_u$  is a subset of paths on the time-extended graph, and  $\emptyset$  represents the option to drop out of the system if the AAM vehicle cannot be allocated to a feasible path due to high congestion. Fig. 2 is a schematic illustrating a time-trajectory scenario for a package delivery drone. Each AAM vehicle  $u \in U(t)$  derives a (private) value  $v_{u,s} \in \mathbb{R}_{\geq 0}$  if it is allocated an option  $s \in M_u$ .

In this work, we develop an efficient algorithm for the SP to allocate airspace regions to AAM vehicles on demand. The algorithm ensures that capacity constraints are respected while eliminating the need for the SP to know the private valuations of the AAM vehicles. In the next subsection, we propose a market-based solution to address the problem of allocating airspace regions to the AAM vehicles.

### 3 Market Mechanisms for Airspace Management

We propose that the service provider (SP) allocates regions to AAM vehicles in a receding horizon manner by periodically gathering demand from UAVs and distributing the available capacity of airspace regions using an auction mechanism (to be defined shortly). In each round of the receding horizon, the SP grants each participating vehicle a certain amount of ‘air credits’, which act as a form of artificial currency for purchasing access to the airspace in that round. Specifically, for any given horizon, the SP assigns each vehicle a budget of  $w_u \geq 0$  air credits<sup>5</sup> to each AAM vehicle  $u$ . The SP charges an anonymous payment of  $p_e$  for the use of each edge  $e \in \tilde{\mathcal{E}}$ . Given these constraints, each AAM vehicle  $u \in U(t)$  selects an option  $s \in M_u$  that maximizes its value under the allocated budget.

If an AAM vehicle is not allocated during a round, it can convert its unused air credits into an “outside option”, denoted by  $\circ$ , for future use. The SP assigns a price  $p_\circ \geq 0$  per unit of the outside option, while the utility that each vehicle derives from this outside option is represented by  $v_{u,\circ} > 0$ .

In what follows, we only focus on one round of the auction mechanism, with the understanding that this mechanism is implemented in a receding horizon manner. The set of AAM vehicles demanding access in one round of auctions is denoted by  $U$ . We define  $x_{u,e} \in \{0, 1\}$  to denote whether an AAM vehicle  $u$  is using edge  $e \in \tilde{\mathcal{E}}$  and  $x_{u,\emptyset} \in \{0, 1\}$  if the AAM vehicle  $u$  has dropped out of the system. Finally, we use

---

<sup>5</sup>The variation in budgets is due to two factors: (i) the SP prioritizing disaster relief and emergency service vehicles, and (ii) the savings individual AAM vehicles accumulate from previous rounds of interaction.

$x_{u,o}$  to denote the amount of outside options that the AAM vehicle consumes for future use. For concise notation, we define  $\mathbf{x}_u = (x_{u,e})_{e \in \tilde{\mathcal{E}}}$  and  $\bar{\mathbf{x}}_u = [\mathbf{x}_u^\top, x_{u,o}, x_{u,\emptyset}]^\top$ . Consequently, the overall utility derived by AAM vehicle  $u$  is given by

$$f_u(\bar{\mathbf{x}}_u) = \sum_{s \in R_u} v_{u,s} x_{u,e^*(s)} + v_{u,o} x_{u,o} + v_{u,\emptyset} x_{u,\emptyset}, \quad (1)$$

where  $e^*(s)$  denotes the *departing edge*<sup>6</sup> on the route  $s$ . Upon observing the price  $\mathbf{p} = (p_e)_{e \in \tilde{\mathcal{E}}}$ , each AAM vehicle solves the following optimization problem:

$$\max_{\mathbf{x}_u} f_u(\bar{\mathbf{x}}_u) \quad (\text{IOP})$$

$$\text{s.t. } \mathbf{p}^\top \mathbf{x}_u + p_o x_{u,o} \leq w_u \quad (2a)$$

$$\tilde{\mathbf{a}}_u^\top \mathbf{x}_u + x_{u,\emptyset} = 1 \quad (2b)$$

$$\tilde{\mathbf{A}}_u \mathbf{x}_u = \mathbf{0} \quad (2c)$$

$$\mathbf{x}_u \in \{0, 1\}^{|\tilde{\mathcal{E}}|}, x_{u,\emptyset} \in \{0, 1\}, \quad (2d)$$

where  $\tilde{\mathbf{a}}_u \in \mathbb{R}^{|\tilde{\mathcal{E}}|}$  is such that the constraint (2b) enforces  $\sum_{s \in R_u} x_{u,e^*(s)} + x_{u,\emptyset} = 1$ , indicating that the AAM vehicle  $u$  will either select a path in  $R_u$  or will drop out. The matrix  $\tilde{\mathbf{A}}_{u,s} \in \mathbb{R}^{K \times (|\tilde{\mathcal{E}}|)}$  in (2c) represents two types of constraints: (i)  $\mathbf{A}_u \mathbf{x}_u = \mathbf{0}$ , where  $\mathbf{A}_u \in \mathbb{R}^{|\tilde{\mathcal{R}}| \times |\tilde{\mathcal{E}}|}$  is an incidence matrix of the time-extended graph encoding flow-balance constraints at each node in  $\tilde{\mathcal{G}}$ ; and (ii)  $\mathbf{B}_{u,s} \mathbf{x}_u = 0$  for each  $s \in R_u$ , where  $\mathbf{B}_{u,s} \in \mathbb{R}^{(K-|\tilde{\mathcal{R}}|) \times |\tilde{\mathcal{E}}|}$  encodes that the flow on any edge connecting two different regions along path  $s$  matches the flow on the departing edge  $e^*(s)$ . Intuitively, (ii) ensures that any feasible solution that satisfies (2b) and (i) results in a unique edge flow. We present a simple example in Section A to describe these constraints.

In (2), (IOP) represents the utility derived by the AAM vehicle  $u$ ; (2a) denotes the budget constraint of AAM vehicle  $u$ ; (2b) represents the requirement that AAM vehicle  $u$  must select at least one of the paths in  $R_u$  or consider dropping out; (2c) ensures a unique edge flow for every feasible solution from (2b); and (2d) ensures that the selections made by AAM vehicles are integral. Note that the feasible set in (2) is non-empty. This is because  $\mathbf{x}_u = \mathbf{0}, x_{u,\emptyset} = 1$ , and  $x_{u,o} = w_u/p_o$  is always a feasible solution.

The goal of the SP is to set the prices such that the resulting allocation is efficient in the following manner: the prices and consumption levels are at a *competitive equilibrium*.

**Definition 3.1.**  $(\bar{\mathbf{x}}^*, \mathbf{p}^*)$  is said to be a competitive equilibrium if the following conditions are satisfied

- (i) For every  $u \in U$ ,  $\bar{\mathbf{x}}_u^*$  is an optimal solution of (2) with price set to  $\mathbf{p}^*$ ;
- (ii) The capacity constraints are satisfied. That is, for every  $e \in \tilde{\mathcal{E}}$ ,  $\sum_{u \in U} x_{u,e}^* \leq \ell_e$ .
- (iii)  $p_e^* \geq 0$  for all  $e \in \tilde{\mathcal{E}}$ ; and if  $p_e^* > 0$  then  $\sum_{u \in U} x_{u,e}^*(p^*) = \ell_e$ .

In general, a competitive equilibrium may not always exist (Budish, 2011). Therefore, we introduce a relaxed version of competitive equilibrium, where we relax the requirement that allocations are integral.

**Definition 3.2.**  $(\bar{\mathbf{x}}^*, \mathbf{p}^*)$  is called the fractional-competitive equilibrium if all conditions in Definition 3.1 are satisfied, except that in Definition 3.1-(i) the integral constraint (2d) is relaxed to a positivity constraint.

<sup>6</sup>In our framework we use the convention that the AAM vehicles place all their valuation of a route on the first edge on the time-extended graph that goes out from the origin node. This is an edge of type  $\tilde{\mathcal{E}}^{(4)}$  in Definition 2.1.



This relaxation is inspired by the competitive equilibrium framework studied in the literature on Fisher markets with linear constraints (Jalota et al., 2023). In the following, we demonstrate that a fractional competitive equilibrium always exists and can be computed as the solution to a fixed-point problem. Finally, in the next section, we leverage this property to develop a two-step algorithmic procedure that produces an integral allocation and prices approximating a competitive equilibrium, without requiring knowledge of the private valuations of the AAM vehicles.

**Existence and Computation of Fractional Competitive Equilibrium** Next, we establish the following existence result:

**Proposition 3.3.** *There exists a fractional-competitive equilibrium.*

The proof builds on the result establishing the existence of a competitive equilibrium in Fisher markets with auxiliary inequality constraints (Jalota et al., 2023). Specifically, our proof accounts for auxiliary *equality* constraints that arise from (2b)-(2c). A detailed proof of Proposition 3.3 is provided in subsection B.1. Next, we present an optimization-based framework to compute a fractional-competitive equilibrium. Consider the following optimization problem, parametrized by  $\omega \in \mathbb{R}_{>0}^{|U|}$ :

$$\max_{\bar{\mathbf{x}}=(\bar{\mathbf{x}}_u)_{u \in U}} \sum_{u \in U} (w_u + \omega_u) \log(f_u(\bar{\mathbf{x}}_u)) - \sum_{u \in U} p_{\circ} x_{u,\circ} \quad (3a)$$

$$\text{s.t.} \quad \sum_{u \in U} x_{u,e} \leq \ell_e \quad \forall e \in \tilde{\mathcal{E}} \quad (3b)$$

$$\tilde{\mathbf{a}}_u^\top \mathbf{x}_u + x_{u,\circ} = 1 \quad (3c)$$

$$\tilde{\mathbf{A}}_u \mathbf{x}_u = \mathbf{0} \quad (3d)$$

$$x_{u,e} \geq 0 \quad \forall u \in U, e \in \tilde{\mathcal{E}} \cup \{\circ, \emptyset\}, \quad (3e)$$

where the first term in (3a) represents the “budget-adjusted” weighted geometric mean of the utilities of all AAM vehicles, while the second term accounts for the total expenditure on the outside option. Constraint (3b) enforces the capacity limit on every edge, and constraints (3c)-(3d) are analogous to (2b)-(2c). Additionally, (3e) is a relaxation of (2d). The objective in (3) is related to the “budget-adjusted social optimization problem” studied in (Jalota et al., 2023) for Fisher markets, with the key difference being the second term, which ensures that a smaller amount of credits is spent on the outside option.

**Lemma 3.4.** *The constraints (3b)-(3e) always have a feasible solution. Furthermore, for any  $\omega \geq \mathbf{0}$ , (3) is a convex optimization problem.*

The proof of this result follows from the fact that the constraint set in (3) is a polytope. Moreover, the objective is a concave function as  $f_u(\cdot)$  is a linear function with positive coefficients.

For any  $\omega \in \mathbb{R}_{\geq 0}^{|U|}$ , let  $\mathbf{p}^\dagger(\omega)$  denote an optimal dual multiplier corresponding to the constraint (3b),  $\lambda^\dagger(\omega)$  denote an optimal dual multiplier corresponding to the constraint (3c), and  $\bar{\mathbf{x}}^\dagger(\omega)$  denote an optimal solution to (3).

**Proposition 3.5.** *Suppose there exists  $\omega^* \in \mathbb{R}_{\geq 0}^{|U|}$  which is a fixed point of the mapping  $\omega \mapsto \lambda^\dagger(\omega)$ . Then  $(\bar{\mathbf{x}}^\dagger(\omega^*), \mathbf{p}^\dagger(\omega^*))$  is a fractional-competitive equilibrium.*

The proof relies on the convexity of the optimization problems (3) (Lemma 3.4) and (2) (after relaxing the constraint (2d) to be fractional), along with matching the KKT conditions for optimality. The detailed proof of Proposition 3.5 is provided in Section B.2.

**Remark 3.6.** *The proof of Proposition 3.5 can be extended to settings where the fixed point may not exist. Suppose there exists  $\omega^* \in \mathbb{R}_{\geq 0}^{|U|}$  such that, for each  $u \in U$ ,  $\omega_u^* - \lambda_u^\dagger(\omega^*) = \epsilon_u$  for some  $\epsilon_u \in \mathbb{R}$  ensuring that  $w_u + \epsilon_u \geq 0$ . Then  $(\bar{\mathbf{x}}^\dagger(\omega^*), \mathbf{p}^\dagger(\omega^*))$  is a fractional-competitive equilibrium of a market where, for each  $u \in U$ , the budget is adjusted to  $w_u + \epsilon_u$ .*

## 4 Algorithm

In this section, we outline our algorithmic procedure for the service provider (SP) to allocate airspace regions efficiently to AAM vehicles, without any knowledge of their private valuations. Our approach unfolds in two stages. First, we introduce an algorithm that solves the fixed-point equation from Proposition 3.5 to compute the fractional-competitive equilibrium in a distributed manner. Next, using the prices and fractional allocations derived from this step, the SP generates a ranked list of AAM vehicles. This ranking allows the SP to achieve an integral allocation by successively assigning regions to AAM vehicles according to the ranking. In the following subsections, we elaborate on each of these steps.

### 4.1 Step 1: Distributed Algorithm for Computing Fractional-Competitive Equilibrium

To compute the fractional-competitive equilibrium, we propose Algorithm 1 to solve the fixed-point problem described in Proposition 3.5 in a distributed manner. Algorithm 1 emulates the fixed-point iteration for the mapping

$$\omega \mapsto \lambda^\dagger(\omega). \quad (\text{FP})$$

Since the SP does not have access to  $\lambda^\dagger(\omega)$  as it does not know the private valuation of AAM vehicles, we employ a two-loop approach. In the inner loop, we iteratively solve the convex optimization problem (3) in a distributed manner that does not require the SP to access the private valuations of AAM vehicles. This is done by repeatedly interacting with the AAM vehicles for finite number of rounds, while holding  $\omega$  constant, to approximate  $\lambda^\dagger(\omega)$ . This approximation is then used to update  $\omega$  in the outer loop.

To solve the inner loop problem in a distributed manner, we reformulate (3) as (4) by introducing two additional variables,  $\mathbf{y}$  and  $\mathbf{z}$ . This reformulation enables the use of distributed optimization techniques, facilitating distributed computation across multiple agents while preserving the structure of the original problem.

$$\min_{(\bar{\mathbf{x}}_u, \mathbf{y}_u)_{u \in U}, (z_e)_{e \in \mathcal{E}}} \sum_{u \in U} (w_u + \omega_u) \log(f_u(\bar{\mathbf{x}}_u)) - \sum_{u \in U} p_{\mathbf{o}} x_{u, \mathbf{o}} \quad (4a)$$

$$\text{s.t. } \mathbf{y}_u = \mathbf{x}_u \quad \forall u \in U, \quad (4b)$$

$$\sum_{u \in U} y_{u, e} + \bar{z}_e = \ell_e \quad \forall e \in \tilde{\mathcal{E}} \quad (4c)$$

$$\tilde{\mathbf{a}}_u^\top \mathbf{x}_u + x_{u,\emptyset} = 1 \quad (4d)$$

$$\tilde{\mathbf{A}}_u \mathbf{x}_u = \mathbf{0} \quad (4e)$$

$$\bar{\mathbf{x}}_u \geq \mathbf{0}, \mathbf{z} \geq \mathbf{0}, \mathbf{y}_u \in \mathbb{R}^{|\tilde{\mathcal{E}}|}, \quad \forall u \in U. \quad (4f)$$

In this reformulation, Equation (4b) enforces equality between  $\mathbf{x}$  and  $\mathbf{y}$ , while Equation (4c) ensures that capacity constraints are met. Constraints (4d)-(4f) are identical to (3c)-(3e) along with additional positivity constraints on  $\mathbf{y}, \mathbf{z}$ . This reformulation ensures that the Lagrangian of (4) becomes a separable function of  $\bar{\mathbf{x}}_u$ , enabling the problem to be solved in a distributed manner using the ADMM algorithm (He et al., 2023; Jalota et al., 2023). The variable  $\mathbf{y}$  can be interpreted as the "baseline demand" expected by the service provider (SP), while  $\mathbf{z}$  represents the "resource surplus" in each region. Next, we describe the inner and outer loop in detail. We index the inner loop iterations by  $n = 1, 2, \dots, N$  and the outer loop iterations by  $k = 1, 2, \dots, K$ .

**Inner Loop:** Given that outer loop is at iteration  $k$ , at any iteration  $n$  of the inner loop: (a) every AAM vehicle  $u$  keeps track its individual demand  $\bar{\mathbf{x}}_u^{(n,k)}$ , and (b) the SP keeps track of three quantities: an estimate of expected baseline demands  $\mathbf{y}^{(n,k)}$ , expected resource surplus  $\mathbf{z}^{(n,k)}$ , price of all regions  $\mathbf{p}^{(n,k)}$ , and a dual multiplier  $\lambda^{(n,k)}$  which is used to adjust budgets of AAM vehicles.

Local update for each AAM vehicle: Given that the outer loop is at iteration  $k$ , at every iteration  $n$  of the inner loop, each AAM vehicle  $u$  receives its expected baseline demand  $\mathbf{y}_u^{(n,k)}$ , the current prices on regions  $\mathbf{p}^{(n,k)}$  and the dual multiplier corresponding to its local constraints  $\lambda_u^{(n,k)}$ . Using this information, AAM vehicle updates its requested demand using the following update and shares this with SP:

$$\begin{aligned} \bar{\mathbf{x}}_u^{(n+1,k)} = \arg \max_{\bar{\mathbf{x}}, \text{ s.t. (3d)-(3e) hold}} & \left( (w_u + \omega_u^{(k)}) \log(f_u(\bar{\mathbf{x}}_u)) - p_{\circ} x_{u,\circ} - \sum_{e \in \tilde{\mathcal{E}}} p_e^{(n,k)} x_{u,e} - \lambda_u^{(n,k)} \cdot (\tilde{\mathbf{a}}_u^\top \mathbf{x}_u + x_{u,\emptyset} - 1) \right. \\ & \left. - \frac{\beta}{2} (\tilde{\mathbf{a}}_u^\top \mathbf{x}_u + x_{u,\emptyset} - 1)^2 - \frac{\beta}{2} \|\mathbf{y}_u^{(n,k)} - \mathbf{x}_u\|^2 \right). \end{aligned} \quad (5)$$

**Remark 4.1.** *The update in Equation (5) can be interpreted as a "proxy bidding agent" used by each AAM vehicle. This proxy attempts to maximize the vehicle's budget-adjusted utility while penalizing deviations from the baseline demand, overspending artificial currency, and violating constraints. These constraints capture the requirement that the bundle of edges selected by the AAM vehicle results in a feasible path on the time-extended graph.*

Updates by SP: Using the demand from AAM vehicles, the SP updates the baseline demand and the excess supply as follows:

$$(\mathbf{y}^{(n+1,k)}, \mathbf{z}^{(n+1,k)}) = \arg \max_{\mathbf{z} \geq \mathbf{0}, \mathbf{y} \in \mathbb{R}^{|\tilde{\mathcal{E}}|}} \left( -\frac{\beta}{2} \|\mathbf{y}_u - \mathbf{x}_u^{(n+1,k)}\|^2 - \frac{\beta}{2} \left\| \sum_{u \in U} \mathbf{y}_u + \mathbf{z} - \ell \right\|^2 - \sum_{e \in \tilde{\mathcal{E}}} p_e^{(n,k)} z_e \right). \quad (6)$$

The objective in (6) requires that SP minimizes three terms: (i) difference between expected baseline demand by SP and the demand sent by AAM vehicles; (ii) constraint violation at the resources; and (iii) unused capacity is minimized on any resource with a positive price. Furthermore, the SP updates the price estimates

using the updated values of baseline demand and excess supply as follows:

$$\mathbf{p}^{(n+1,k)} = \mathbf{p}^{(n,k)} + \beta \left( \sum_{u \in U} \mathbf{y}_u^{(n+1,k)} + \mathbf{z}^{(n+1,k)} - \ell \right). \quad (7)$$

The above equations resemble the idea that an SP should increase the price if the capacity constraint is violated and reduce it if there is available capacity. Finally, the SP updates the dual multiplier estimate  $\lambda_u$ , for every AAM vehicle  $u$  as follows:

$$\lambda_u^{(n+1,k)} = \lambda_u^{(n,k)} + \beta \left( \tilde{\mathbf{a}}_u^\top \mathbf{x}_u^{(n+1,k)} + x_{u,\emptyset}^{(n+1,k)} - 1 \right), \quad (8)$$

which keeps track of flow constraint violations by every agent.

**Outer loop.** In the outer loop, we update the budget adjustment after every  $N$  iteration of the inner loop, using the value of  $\lambda^{(N,k)}$  to approximate the fixed-point iteration (line 12 of Algorithm 1). This step ensures that budget adjustments progressively converge toward the equilibrium by iteratively refining the dual variables based on the current solution from the inner loop.

**Termination criterion:** We terminate the algorithm once **all** of the following errors fall below a predefined threshold:

- Market clearing error (MCE): Smaller values of MCE ensure that resources with a positive price maintain a balance between demand and supply, while resources priced at zero satisfy capacity constraints. We define

$$\text{MCE}(\bar{\mathbf{x}}, \mathbf{p}) = \sqrt{\sum_{e \in \tilde{\mathcal{E}}: p_e > 0} (z_e)^2 + \sum_{e \in \tilde{\mathcal{E}}: p_e = 0} (\max\{0, z_e\})^2}, \quad (9)$$

where  $z_e = \sum_{u \in U} x_{u,e} - \ell_e$  is the *over demand*.

- Individual constraint error (ICE): Smaller values of ICE ensure that (4d) constraint is satisfied. We define

$$\text{ICE}(\bar{\mathbf{x}}) = \sqrt{\sum_{u \in U} (\tilde{\mathbf{a}}_u^\top \mathbf{x}_u + x_{u,\emptyset} - 1)^2}. \quad (10)$$

- Baseline demand error (BDE): Smaller value of BDE ensure that (4b) is satisfied. We define

$$\text{BDE}(\mathbf{x}, \mathbf{y}) = \sqrt{\sum_{u \in U} \|\mathbf{y}_u - \mathbf{x}_u\|_2^2}. \quad (11)$$

We represent the output of Algorithm 1 by  $(\bar{\mathbf{x}}^\dagger, \mathbf{p}^\dagger)$ .

## 4.2 Step 2: Computing Integral Allocation

Using the fractional allocations from Algorithm 1, the service provider (SP) computes an integral allocation in a distributed manner using Algorithm 2. The SP sets the airspace price to  $\mathbf{p}^\dagger$  (the output of Algorithm 1)

---

**Algorithm 1** Distributed Algorithm for Fractional Competitive Equilibrium
 

---

```

1: Input:  $\mathbf{p}^{(0)} = \mathbf{0}, \lambda^{(0)} = \mathbf{0}, \mathbf{y}^{(0)} = \mathbf{0}, \omega^{(0)} = \mathbf{0}, \text{tol}$ 
2: for  $k = 1, 2, \dots, K$  do
3:   for  $n = 0, 1, \dots, N - 1$  do
4:     Upon observing  $\mathbf{p}^{(n,k)}, \mathbf{y}^{(n,k)}, \omega_u^{(k)}$ , each AAM vehicle independently updates its demand
       using (5)
5:     Upon observing  $\bar{\mathbf{x}}_u^{(n,k)}$ , SP updates the baseline demand and overdemand using (6)
6:     SP updates the price estimates using (7)
7:     SP tracks the dual multiplier estimate corresponding to  $\omega^{(k)}$  using (8)
8:     if  $\max\{\text{MCE}(\bar{\mathbf{x}}^{(n,k)}, \mathbf{p}^{(n,k)}), \text{ICE}(\bar{\mathbf{x}}^{(n,k)}), \text{BDE}(\mathbf{x}^{(n,k)}, \mathbf{y}^{(n,k)})\} \leq \text{tol}$  then
9:       Return $(\bar{\mathbf{x}}^{(n,k)}, \mathbf{p}^{(n,k)})$ 
10:    end if
11:  end for
12:   $\omega^{(k+1)} = \lambda^{(N,k)}$ 
13:   $\mathbf{p}^{(0,k+1)} \leftarrow \mathbf{p}^{(N,k)}, \mathbf{y}^{(0,k+1)} \leftarrow \mathbf{y}^{(N,k)}$ 
14: end for

```

---

and generates a *ranked list* of AAM vehicles based on  $\bar{\mathbf{x}}^\dagger$ . This list is created by ranking the AAM vehicles in descending according to the value of the (fractional) allocation of their preferred routes.

*Ranked List:* More formally, define  $s^*(u)$  to denote the most desired route of AAM vehicle  $u$  in  $R_u$ . The SP creates a ranking over agents based on decreasing values of  $x_{u,e^*(s^*(u))}^\dagger$ , where  $e^*(s^*(u))$  denotes the departing edge on the route  $s^*(u)$ . We denote the ranked list<sup>7</sup> of AAM vehicles by **rank**.

*Integral Allocation:* The SP goes over each AAM vehicle as per their order in **rank** and retrieves the most desired route for each vehicle (determined by solving the individual optimization problem (2)). If any capacity constraints are violated at a resource along the route, the SP either removes that resource from the available pool for all remaining agents or, alternatively, increases the price of that resource to infinity for the remaining AAM vehicles (as described in line 13 of Algorithm 2).

**Remark 4.2.** *Note that in Algorithms 1-2, the SP does not require any information about the private valuations of individual AAM vehicles. Furthermore, each AAM vehicle is unable to infer the demand or private valuations of other vehicles in the airspace, ensuring that privacy is preserved. The iterative update in (5) can be interpreted as a learning mechanism, where AAM vehicles adapt to the environment based on signals received from the SP, progressively refining their demand through this distributed learning process.*

## 5 Drone Delivery in Toulouse: A Case Study

In this section, we validate our proposed mechanism using a dataset of simulated package deliveries by Airbus, as shown in Fig. 3. Particularly, we use a package delivery scenario where four suppliers in Toulouse, France, have warehouses on the periphery of the city and make deliveries in locations randomly distributed around the city. In the Airbus dataset, the demand is generated using a Poisson process. Each demand simulates delivery operations, where a UAV departs from a specific vertiport, navigates through different sectors, and returns to its original departure vertiport. The trajectory of every UAV is generated using a

---

<sup>7</sup>ties are broken arbitrarily.

---

**Algorithm 2** Ranking System

---

```
1: Input:  $\mathbf{p}^\dagger$ ,  $\mathbf{rank}$ 
2: for  $i = 1$  to  $|U|$  do
3:    $u \leftarrow \mathbf{rank}_i$ 
4:    $\text{AAM\_vehicle\_allocated} = \text{False}$ 
5:   while  $\text{AAM\_vehicle\_allocated} = \text{False}$  do
6:     AAM vehicle  $u$  reports  $\bar{\mathbf{x}}_u$  by solving (2)
7:     if  $x_{u,e} \leq l_e$  for every  $e \in \tilde{\mathcal{E}}$  then
8:       Update available capacity of regions:  $l \leftarrow l - \mathbf{x}_u$ 
9:        $\text{AAM\_vehicle\_allocated} = \text{True}$ 
10:    else
11:       $\text{Contested\_goods} = \{e \in \tilde{\mathcal{E}} \mid x_{u,e} > l_e\}$ 
12:      For every  $e \in \text{Contested\_goods}$ ,  $p_e \leftarrow \inf$ 
13:    end if
14:  end while
15: end for
```

---

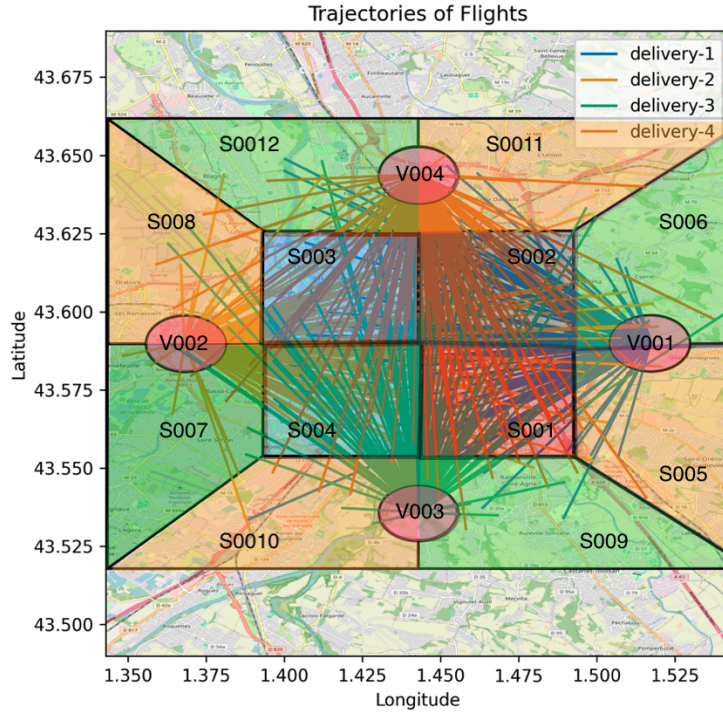


Figure 3: Division of Toulouse airspace into 12 cruising sectors (polygons) and 4 launch-pad sectors (circles). The lines show the trajectory of UAVs in the dataset. Labels indicate the sector (S#) or vertiport (V#).

high-fidelity Airbus trajectory simulator which includes takeoff, cruise, and landing phases. While in the current simulation, the UAV returns to its original departure vertiport, our algorithm can accommodate a return to a different location. Trajectories last approximately 5 minutes staggered at different departing times to simulate a realistic operational system. The entire simulation provides 4,000 seconds of simulated flight data. For our analysis, we divide the city into 12 cruising regions and 4 vertiports regions, as shown in Fig. 3.

Each flight has a desired 4D trajectory (three spatial dimensions with time as the fourth dimension). We assign a uniformly random utility to each flight between 150 and 250. The utility for each flight is highest when it can depart and arrive at its *preferred times*, with the utility decreasing by a factor of  $\delta = 0.95$  for each time step delay in departure time. We consider the value agents get from the outside option of 1 and from dropping out 40. The preferred menu for every agent is to stay parked for a small valuation, take the highest utility path, or delay for up to four steps.

We implement our mechanism (Algorithms 1-2) in three receding horizon steps of the Toulouse example, scheduling auctions at 5-minute intervals. Each time unit in our simulation represents 15 seconds; therefore, 20 units of time between horizon steps correspond to 5 minutes between rounds. Before the start, the SP assigns each agent a per-auction budget of air credits to all participating vehicles, between 150 and 250, which they have access to for each round. Before the start of every round, the SP gathers the demand for AAM vehicles requesting access to airspace. The overall budget of any UAV is comprised of the new air credits they received and any remaining budget from a previous round.

In Fig. 4, we present the evolution of prices and congestion across various sectors overtime during the first three auctions of the Toulouse example. Only the sectors with non-zero prices at some point are included, and we observe that capacity constraints are consistently met in all sectors. In the top plot, three sectors show positive prices in at least one of the auctions, with these prices corresponding to times of maximum sector utilization, as illustrated in the second plot<sup>8</sup>. An interesting observation in the first plot is that prices for sector S004 become positive only during the third auction, despite some drones being allocated to it for future use as early as the first auction (between 0 and 20 time units). Sector S004, however, only reaches maximum capacity during the third auction, resulting in the observed positive prices. Additionally, the prices for sectors S001 and S002 before and around time step 40 are considerably higher than any agent’s budget, which might initially appear inconsistent with five agents being allocated to these sectors at that time, as shown in the second plot. However, these agents were actually allocated in the first auction, when prices were low, as indicated by the solid line in the first plot. The subsequent high prices are reasonable because the sectors are at maximum capacity and cannot accommodate new requests in auctions 2 and 3. The third plot in Fig. 4 shows non-zero prices for certain departure and arrival slots. Overall, our mechanism effectively maintains congestion below the respective thresholds for all sectors, vertiports, and take-off/landing slots—at 5, 10, and 1—despite requests that exceed these capacities.

In Fig. 5, we present the evolution of various errors resulting from Algorithm 1 in the first auction round. First, in Fig. 5a, we analyze the evolution of the fixed point error,  $\|\lambda^{(n,k)} - \omega^{(k)}\|$ , as both  $n$  and  $k$  increase within Algorithm 1. Here, the inner loop length is set to  $N = 20$ . The fixed point error consistently decreases with additional inner loop rounds, suggesting a contraction property in the fixed point map (FP). Further research could explore sufficient conditions that ensure this contraction in relation to the underlying

---

<sup>8</sup>Recall our market clearing definition: congestion can reach a maximum in a sector even if prices are zero.

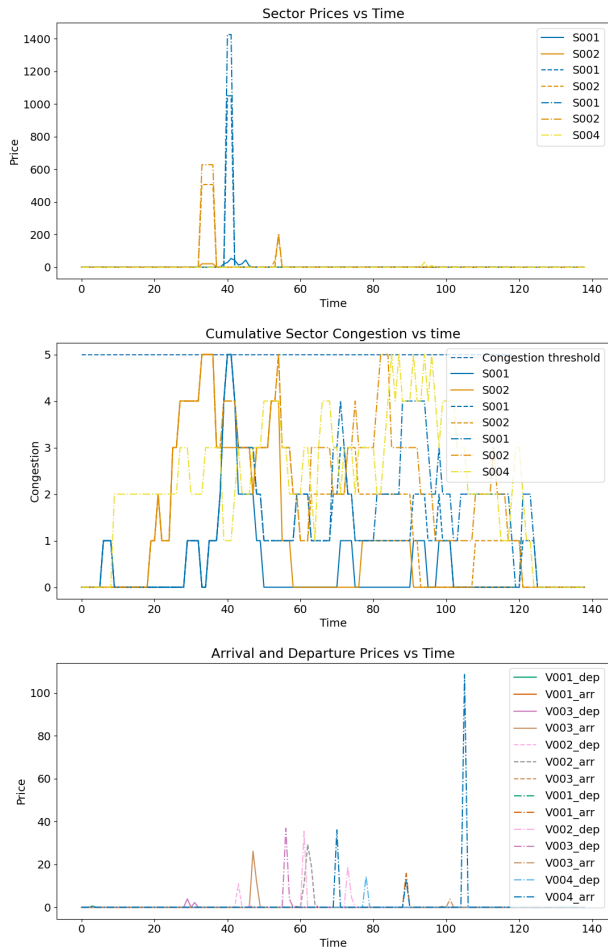


Figure 4: Evolution of prices and congestion of various sectors with time for the first three auctions of the Toulouse example. Only goods with non-zero prices are included. Regular lines, dashed lines, and dot-dashed lines denote the results of the 1st, 2nd, and 3rd auctions, respectively. The figure only includes goods where the price is non-zero at some timestamp. a) Price of goods vs time shows some positive prices for sectors 1, 2, and 4. b) Cumulative sector congestion shows the total allocated airspace after each auction, including airspace that was allocated in a previous auction. c) The price of arrival and departure slots shows positive prices for some arrival slots.



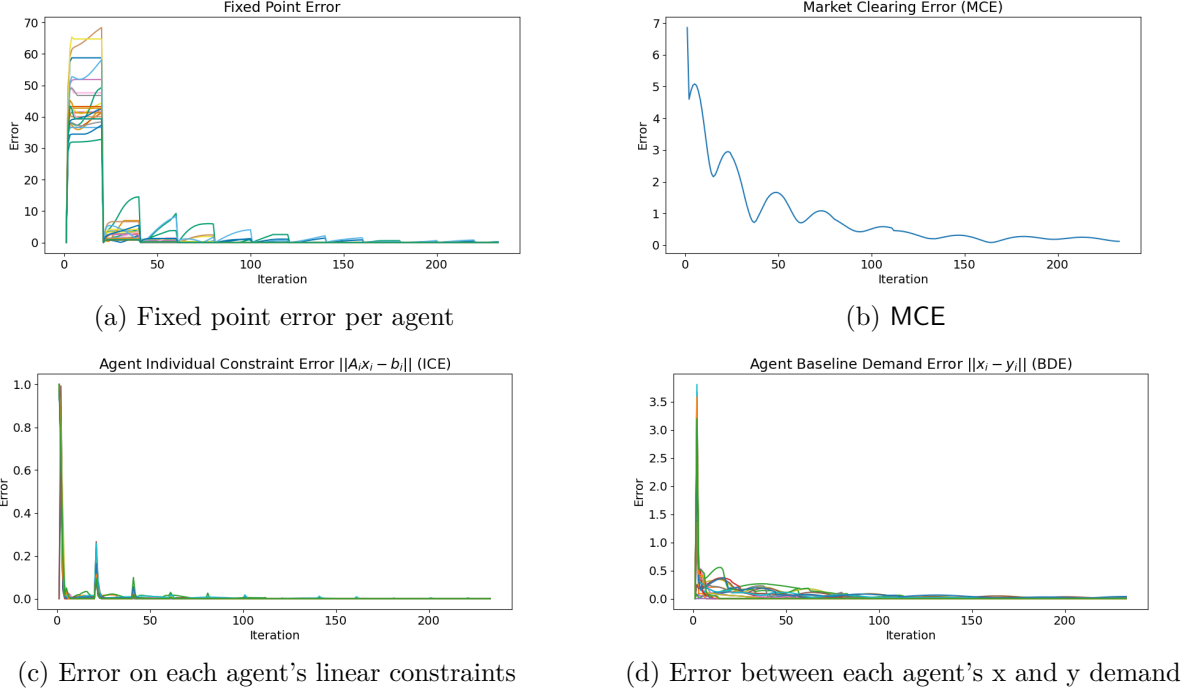


Figure 5: Convergence of Error Terms

AAM market parameters. In Fig. 5b, we present the evolution of the market clearing error (MCE, defined in (9)), which ultimately approaches zero. This indicates that resources with positive prices achieve a balance between demand and supply, while zero-priced resources satisfy capacity constraints. In Fig. 5c, we show the evolution of the individual constraint error (ICE, defined in (10)), which also converges to zero, indicating satisfaction of (4e). Notably, we observe spikes at the start of each inner loop due to updates in the budget adjustment parameter, which alter the outcome of (5). Lastly, in Fig. 5d, we present the evolution of the baseline demand error (BDE, defined in (11)), which also converges to zero, confirming that (4b) is met. This analysis highlights Algorithm 1’s effectiveness in reducing errors and satisfying key constraints within the auction framework.

## 6 Vertiport Reservation Mechanism in Northern California

In this section, we study a scenario of vertiport reservation for (hypothesized) air taxi services in Northern California. We simulate a scenario where different air taxis request access to air routes to transport people at an urban and regional level. The vertiports in this simulation are located in various cities in Northern California as shown in the map in Fig. 6. For simplicity, we are modeling linear trajectories and assuming a maximum travel range of 100 miles.

In this example, 20 air taxis request a departure, air route, and landing clearances among seven vertiport destinations during a 10-minute auction window. The requests by the air taxis, the final allocation of routes, and payments to the SP are presented in Table 1. Additional information from the network in Table 2 displays the maximum capacity in every segment of the desired routes, the utility of the air taxis for a given path, and their initial air credits. We set  $\beta = 50, p_o = 10, v_{u,o} = 1, v_{u,\emptyset} = 1, N = 2, \text{tol} = 1 \times 10^{-4}$ .

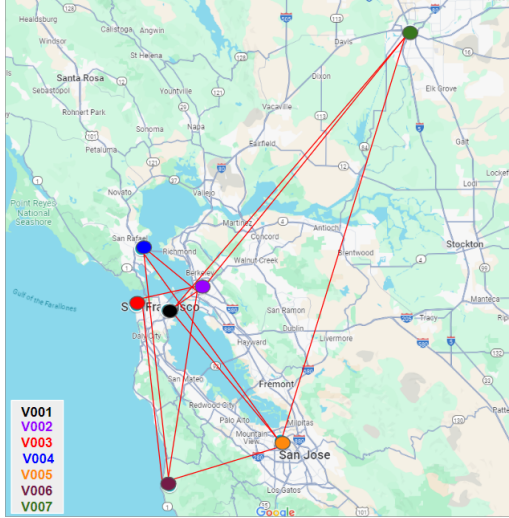


Figure 6: Northern California Vertiport Map. This map, based on an image from Google Maps, highlights seven distinct vertiports with unique color codes, showing the example routes in red lines for clarity.

In these tables, air taxis marked with the same color indicate that they demanded the same trajectory slot simultaneously, resulting in a constraint violation. Consequently, only a subset of these air taxis were allocated their preferred route, while others were denied access.

Below, we highlight the main observations from our numerical study.

- (i) At time step 16, AC003, AC004, and AC015 request departure from V002, which has a departure capacity constraint of one. Consequently, only AC004 is allocated to depart at this time step due to its higher air credits, while AC003 and AC015 are delayed. Naturally, these air taxis would prefer to depart at the next time step; however, they now compete for departure from V002 with AC013 and AC018 at time steps 17 and 18, respectively. Notably, Algorithm 2 prioritizes AC013 and AC018, resulting in further delays for AC003 and AC015. At time step 19, AC003 and AC015 compete again, with AC003 receiving priority due to its higher air credits in Algorithm 2.
- (ii) AC002 and AC011 request landing slots at V004 at the same time, which results in delay for AC011. This is because AC011 has both a lower budget and lower utility in comparison to AC002.
- (iii) AC009 and AC010 request departure from V001 at the same time, which results in delay for AC009. This is because AC010 has a significantly higher budget than AC009.
- (iv) Air taxis that are delayed are charged less than those who are allocated their preferred routes.

## 7 Conclusions

In this work, we introduce a novel mechanism that enables service providers to allocate on-demand requests from Advanced Air Mobility (AAM) vehicles, each with heterogeneous private valuations, to a capacity-constrained airspace. We evaluate the effectiveness of our approach using a physically accurate urban air delivery dataset and hypothesized electric air-taxi services in Northern California.

Table 1: Allocation of air taxis to the desired route and the corresponding payments

Agent	Req. Route	Req. (Dep, Arr)	Allocated (Dep, Arr)	Status	Payment (\$)
AC001	(V007, V002)	(16, 54)	(16, 54)	on-time	0.0
AC002	(V005, V004)	(19, 47)	(19, 47)	on-time	5.73
AC011	(V006, V004)	(19, 47)	(20, 48)	delayed	1.53
AC003	(V002, V001)	(16, 21)	(19, 24)	delayed	3.71
AC004	(V002, V001)	(16, 21)	(16, 21)	on-time	20.36
AC015	(V002, V001)	(16, 21)	(20, 25)	delayed	0.86
AC013	(V002, V006)	(17, 41)	(17, 41)	on-time	11.11
AC018	(V002, V007)	(18, 56)	(18, 56)	on-time	8.46
AC005	(V003, V002)	(11, 19)	(11, 19)	on-time	0.0
AC006	(V005, V007)	(18, 68)	(18, 68)	on-time	0.0
AC007	(V003, V002)	(15, 23)	(15, 23)	on-time	0.0
AC008	(V007, V001)	(12, 54)	(12, 54)	on-time	0.0
AC009	(V001, V005)	(13, 34)	(14, 35)	delayed	2.10
AC010	(V001, V005)	(13, 34)	(13, 34)	on-time	5.75
AC012	(V005, V001)	(16, 37)	(16, 37)	on-time	0.0
AC014	(V001, V002)	(11, 24)	(11, 24)	on-time	0.0
AC016	(V007, V005)	(17, 67)	(17, 67)	on-time	0.0
AC017	(V004, V006)	(16, 44)	(16, 44)	on-time	0.0
AC019	(V004, V002)	(16, 35)	(16, 35)	on-time	0.0
AC020	(V003, V006)	(16, 38)	(16, 38)	on-time	0.11

Our findings suggest several promising directions for future research. First, deriving formal guarantees regarding the neighborhood within which the fixed point operator (FP) is contractive, based on AAM market parameters, would be crucial for establishing theoretical convergence guarantees for our algorithmic approach, which has shown strong performance in simulations. Additionally, exploring formal incentive compatibility and fairness guarantees within the proposed allocation mechanism presents an exciting area for further study.

## 8 Acknowledgments

Chinmay Maheshwari, Pan-Yang Su, and Shankar Sastry acknowledge support from NSF Collaborative Research: Transferable, Hierarchical, Expressive, Optimal, Robust, Interpretable NETWORKS (THEORINET) Award No. DMS 2031899. Victoria Tuck and Shankar Sastry acknowledge support from Provably Correct Design of Adaptive Hybrid Neuro-Symbolic Cyber-Physical Systems, Defense Advanced Research Projects Agency award number FA8750-23-C-0080. Maria G. Mendoza and Shankar Sastry acknowledge support from NASA, Clean Sheet Airspace Operating Design project award number MFRA2018-S-0471. Victor L Qin was supported by the National Science Foundation Graduate Research Fellowship Program under Grant No. 2141064. Any opinions, findings, conclusions, or recommendations expressed in this material are those of the author(s) and do not necessarily reflect the views of the National Science Foundation.

Table 2: Utility and air-credits for different air taxis, along with the capacity constraints on their route

Aircraft	Routes	Max. Capacity (Dep, Route, Arr)	Initial Air Credits	Utility	Status	Rank
AC001	(V007, V002)	(2,4,1)	125	118	on-time	6
AC002	(V005, V004)	(4,5,1)	90	171	on-time	7
AC011	(V006, V004)	(1,2,1)	78	135	delayed	19
AC003	(V002, V001)	(1,1,2)	135	172	delayed	18
AC004	(V002, V001)	(1,1,2)	154	133	on-time	13
AC015	(V002, V001)	(1,1,2)	65	194	delayed	20
AC013	(V002, V006)	(1,4,3)	55	147	on-time	16
AC018	(V002, V007)	(1,2,3)	103	165	on-time	8
AC005	(V003, V002)	(1,5,1)	83	177	on-time	4
AC006	(V005, V007)	(4,3,3)	199	148	on-time	15
AC007	(V003, V002)	(1,5,1)	100	183	on-time	5
AC008	(V007, V001)	(2,3,2)	104	155	on-time	10
AC009	(V001, V005)	(5,1,2)	67	189	delayed	17
AC010	(V001, V005)	(5,1,2)	114	163	on-time	3
AC012	(V005, V001)	(4,3,2)	90	124	on-time	12
AC014	(V001, V002)	(5,2,1)	64	174	on-time	9
AC016	(V007, V005)	(2,5,2)	109	189	on-time	14
AC017	(V004, V006)	(5,3,3)	155	149	on-time	11
AC019	(V004, V002)	(5,5,2)	104	147	on-time	1
AC020	(V003, V006)	(1,2,3)	96	146	on-time	2

## References

- Federal Aviation Administration. Unmanned aircraft system (uas) traffic management (utm) concept of operations (conops) version 2.0. [https://www.faa.gov/sites/faa.gov/files/2022-08/UTM\\_ConOps\\_v2.pdf](https://www.faa.gov/sites/faa.gov/files/2022-08/UTM_ConOps_v2.pdf), 2022.
- Lawrence M. Ausubel and Peter Cramton. Auctioning Many Divisible Goods. *Journal of the European Economic Association*, 2(2-3):480–493, 05 2004. ISSN 1542-4766. doi: 10.1162/154247604323068168. URL <https://doi.org/10.1162/154247604323068168>.
- Lawrene M. Ausubel and Paul Milgrom. The lovely but lonely vickrey auction. Discussion Papers 03-036, Stanford Institute for Economic Policy Research, 2004. URL <https://EconPapers.repec.org/RePEc:sip:dpaper:03-036>.
- Hamsa Balakrishnan and Bala Chandran. A distributed framework for traffic flow management in the presence of unmanned aircraft. ATM Seminar, 2017.
- Michael O. Ball, Frank Berardino, and Mark Hansen. The use of auctions for allocating airport access rights. *Transportation Research Part A: Policy and Practice*, 114:186–202, 2018. ISSN 0965-8564. doi: <https://doi.org/10.1016/j.tra.2017.09.026>. URL <https://www.sciencedirect.com/science/article/pii/S0965856416303287>.
- Michael O. Ball, Alexander S. Estes, Mark Hansen, and Yulin Liu. Quantity-contingent auctions and allocation of airport slots. *Transportation Science*, 54(4):858–881, 2020. doi: 10.1287/trsc.2020.0995. URL <https://doi.org/10.1287/trsc.2020.0995>.
- Aleksandar Bauranov and Jasenka Rakas. Designing airspace for urban air mobility: A review of concepts and approaches. *Progress in Aerospace Sciences*, 125:100726, 2021. ISSN 0376-0421. doi: <https://doi.org/10.1016/j.paerosci.2021.100726>. URL <https://www.sciencedirect.com/science/article/pii/S0376042121000312>.
- Dimitris Bertsimas and Sarah Stock Patterson. The air traffic flow management problem with enroute capacities. *Operations Research*, 46(3):406–422, 1998. doi: 10.1287/opre.46.3.406. URL <https://doi.org/10.1287/opre.46.3.406>.
- Dimitris Bertsimas and Sarah Stock Patterson. The traffic flow management rerouting problem in air traffic control: A dynamic network flow approach. *Transportation Science*, 34(3):239–255, 2000. doi: 10.1287/trsc.34.3.239.12300. URL <https://doi.org/10.1287/trsc.34.3.239.12300>.
- Dimitris Bertsimas, Guglielmo Lulli, and Amedeo Odoni. An integer optimization approach to large-scale air traffic flow management. *Operations Research*, 59(1):211–227, 2011. doi: 10.1287/opre.1100.0899. URL <https://doi.org/10.1287/opre.1100.0899>.
- Eric Budish. The combinatorial assignment problem: Approximate competitive equilibrium from equal incomes. *Journal of Political Economy*, 119(6):1061–1103, 2011. ISSN 00223808, 1537534X. URL <http://www.jstor.org/stable/10.1086/664613>.

- Eric Budish, Ruiquan Gao, Abraham Othman, Aviad Rubinstein, and Qianfan Zhang. Practical algorithms and experimentally validated incentives for equilibrium-based fair division (a-ceed). In *Proceedings of the 24th ACM Conference on Economics and Computation*, EC '23, page 337–368, New York, NY, USA, 2023. Association for Computing Machinery. ISBN 9798400701047. doi: 10.1145/3580507.3597809. URL <https://doi.org/10.1145/3580507.3597809>.
- Christopher Chin, Victor Qin, Karthik Gopalakrishnan, and Hamsa Balakrishnan. Traffic management protocols for advanced air mobility. *Frontiers in Aerospace Engineering*, 2:1176969, 2023.
- Peter Cramton, Yoav Shoham, and Richard Steinberg. Introduction to combinatorial auctions. *Combinatorial auctions*, pages 1–14, 2006a.
- Peter C Cramton, Yoav Shoham, Richard Steinberg, and Vernon L Smith. *Combinatorial auctions*, volume 1. MIT press Cambridge, 2006b.
- European Organisation for the Safety of Air Navigation (EUROCONTROL). U-space ConOps (edition 3.10): U-space capabilities and services to enable Urban Air Mobility. Technical report, EUROCONTROL, July 2022.
- Federal Aviation Administration. Urban Air Mobility (UAM) Concept of Operations Version 2.0. Technical report, Federal Aviation Administration, Washington, DC, April 2023.
- Jingqiu Guo, Long Chen, Lingxi Li, Xiaoxiang Na, Ljubo Vlacic, and Fei-Yue Wang. Advanced air mobility: An innovation for future diversified transportation and society. *IEEE Transactions on Intelligent Vehicles*, 9(2):3106–3110, 2024. doi: 10.1109/TIV.2024.3377464.
- Bingsheng He, Shengjie Xu, and Xiaoming Yuan. Extensions of admm for separable convex optimization problems with linear equality or inequality constraints. In *Handbook of Numerical Analysis*, volume 24, pages 511–557. Elsevier, 2023.
- Devansh Jalota, Marco Pavone, Qi Qi, and Yinyu Ye. Fisher markets with linear constraints: Equilibrium properties and efficient distributed algorithms. *Games and Economic Behavior*, 141:223–260, 2023.
- Christopher Leet and Robert A. Morris. *Combinatorial Auction-Based Strategic Deconfliction of Federated UTM Airspace*. doi: 10.2514/6.2024-4454. URL <https://arc.aiaa.org/doi/abs/10.2514/6.2024-4454>.
- Amedeo R. Odoni. The flow management problem in air traffic control. In Amedeo R. Odoni, Lucio Bianco, and Giorgio Szegö, editors, *Flow Control of Congested Networks*, pages 269–288, Berlin, Heidelberg, 1987. Springer Berlin Heidelberg. ISBN 978-3-642-86726-2.
- Victor Qin and Hamsa Balakrishnan. Cost-aware congestion management protocols for advanced air mobility. 2022.
- Kaushik Roy and Claire J. Tomlin. Solving the aircraft routing problem using network flow algorithms. In *2007 American Control Conference*, pages 3330–3335, 2007. doi: 10.1109/ACC.2007.4282854.

Sven Seuken, Paul Friedrich, and Ludwig Dierks. Market design for drone traffic management. In *Proceedings of the AAAI Conference on Artificial Intelligence*, volume 36, pages 12294–12300, 2022.

Brent Skorup. Auctioning airspace. *NCJL & Tech.*, 21:79, 2019.

Pan-Yang Su, Chinmay Maheshwari, Victoria Tuck, and Shankar Sastry. Incentive-compatible vertiport reservation in advanced air mobility: An auction-based approach, 2024. URL <https://arxiv.org/abs/2403.18166>.

Hal R Varian. Equity, envy, and efficiency. *Journal of Economic Theory*, 9(1):63–91, 1974. ISSN 0022-0531. doi: [https://doi.org/10.1016/0022-0531\(74\)90075-1](https://doi.org/10.1016/0022-0531(74)90075-1). URL <https://www.sciencedirect.com/science/article/pii/0022053174900751>.

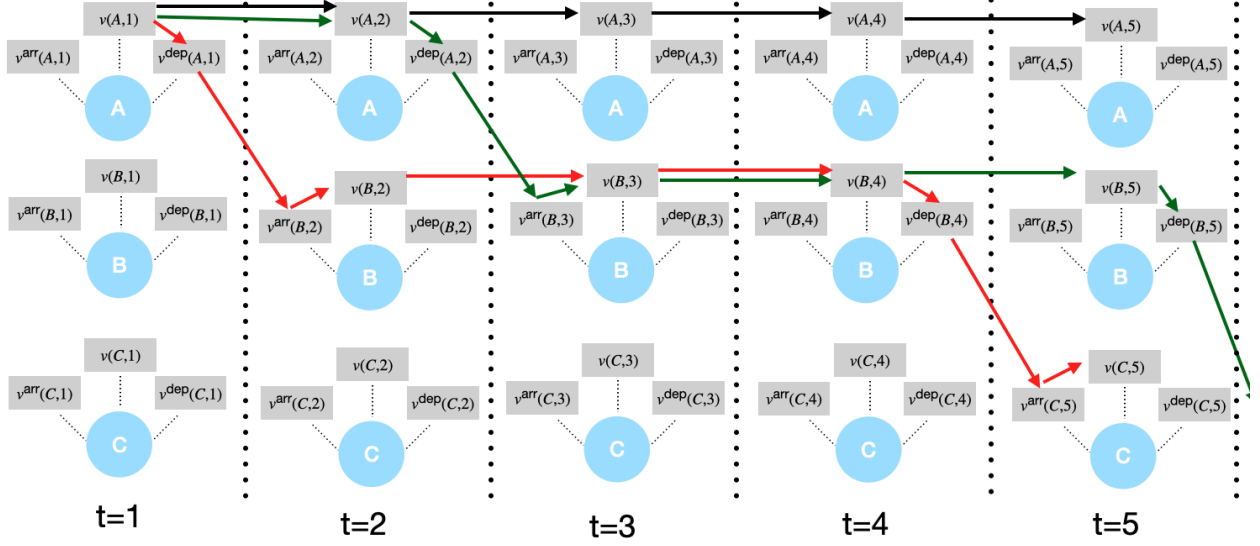


Figure 7: Time Extended Graph: From left to right, we show a sequence of time steps and different color-coded trajectories that an AAM vehicle can request. The red trajectory shows an AAM vehicle traveling from region A to C while transiting from region B. The green trajectory represents the same trajectory as the red path but is delayed by one unit of time. The black trajectory denotes an option where the AAM vehicle stays parked at the origin region. To simplify the visualization, we have not shown all possible edges on this time-extended graph.

## A A Simple Example

In this section, we explain the time-extended graph (Definition 2.1) along with constraints (2b)-(2c) through a simple example comprising of 3 regions, denoted by  $\{A, B, C\}$ .

**Time-extended graph** The time-extended graph (for  $T = 5$ ) corresponding to our scenario is shown in Figure 7. In the time-extended graph  $\tilde{\mathcal{G}} = (\tilde{\mathcal{R}}, \tilde{\mathcal{E}})$ , at every time  $t$  each region  $r$  is replicated into three regions  $t : v(r, t), v^{\text{arr}}(r, t), v^{\text{dep}}(r, t)$ . For conciseness, we will only discuss one edge corresponding to each of the four types  $\tilde{\mathcal{E}}^{(1)}, \tilde{\mathcal{E}}^{(2)}, \tilde{\mathcal{E}}^{(3)}, \tilde{\mathcal{E}}^{(4)}$ . The (red) edge  $(v^{\text{arr}}(B, 2), v(B, 2))$  is an edge of type  $\tilde{\mathcal{E}}^{(1)}$ . The (red) edge  $(v(A, 1), v^{\text{dep}}(A, 1))$  is an edge of type  $\tilde{\mathcal{E}}^{(2)}$ . The (black) edge  $(v(A, 1), v(A, 2))$  is an edge of type  $\tilde{\mathcal{E}}^{(3)}$ . The (green) edge  $(v^{\text{dep}}(A, 2), v^{\text{arr}}(B, 3))$  is an edge of type  $\tilde{\mathcal{E}}^{(4)}$ .

**Constraint (2b)-(2c)** Here, we illustrate the constraints (2b)-(2c) through an example. Consider an AAM vehicle  $u$  that wants to travel from region A to region C. Suppose the menu of that AAM vehicle is comprised of the routes  $s_1, s_2, s_3$ , as described below:

$$s_1 = \{(v(A, 1), v(A, 2)), (v(A, 2), v(A, 3)), (v(A, 3), v(A, 4)), (v(A, 4), v(A, 5))\} \text{ Black-path in Figure 7}$$

$$s_2 = \{(v(A, 1), v^{\text{dep}}(A, 1)), (v^{\text{dep}}(A, 1), v^{\text{arr}}(B, 2)), (v^{\text{arr}}(B, 2), v(B, 2)), (v(B, 2), v(B, 3)), (v(B, 3), v(B, 4)), \\ (v(B, 4), v^{\text{dep}}(B, 4)), (v^{\text{dep}}(B, 4), v^{\text{arr}}(C, 5)), \\ (v^{\text{arr}}(C, 5), v(C, 5))\} \text{ red-path in Figure 7}$$

$$s_3 = \{(v(A, 1), v(A, 2)), (v(A, 2), v^{\text{dep}}(A, 2)), (v^{\text{dep}}(A, 2), v^{\text{arr}}(B, 3)), (v^{\text{arr}}(B, 3), v(B, 3)),$$



$$(v(B, 3), v(B, 4)), (v(B, 4), v(B, 5)), (v(B, 5), v^{\text{dep}}(B, 5)), \\ (v^{\text{dep}}(B, 5), v^{\text{arr}}(C, 6))\} \text{ green-path in Figure 7}$$

Here  $e^*(s_1) = (v(A, 1), v(A, 2))$ ,  $e^*(s_2) = (v(A, 1), v(A, 1)^{\text{dep}})$ ,  $e^*(s_3) = (v(A, 2), v^{\text{dep}}(A, 2))$ . The menu  $M_u$  of AAM vehicle  $u$  is given by  $M_u = \{s_1, s_2, s_3, \emptyset\}$ .

Consequently, the constraint (2b) for this AAM vehicle is given by  $x_{u, e^*(s_1)} + x_{u, e^*(s_2)} + x_{u, e^*(s_3)} + x_{u, \emptyset} = 1$ . Additionally, the constraint (2c) for this AAM vehicle contains two types of constraints: (1) the flow balance constraints:

$$\begin{aligned} x_{u, (v(A, 1), v(A, 2))} &= x_{u, (v(A, 2), v^{\text{dep}}(A, 2))} + x_{u, (v(A, 2), v(A, 3))} \\ x_{u, (v(A, 2), v(A, 3))} &= x_{u, (v(A, 3), v(A, 4))} \\ x_{u, (v(A, 3), v(A, 4))} &= x_{u, (v(A, 4), v(A, 5))} \\ x_{u, (v(A, 2), v^{\text{dep}}(A, 2))} &= x_{u, (v^{\text{dep}}(A, 2), v^{\text{arr}}(B, 3))} \\ x_{u, (v^{\text{dep}}(A, 2), v^{\text{arr}}(B, 3))} &= x_{u, (v^{\text{arr}}(B, 3), v(B, 3))} \\ x_{u, (v^{\text{arr}}(B, 3), v(B, 3))} + x_{u, (v(B, 2), v(B, 3))} &= x_{u, (v(B, 3), v(B, 4))} \\ x_{u, (v(B, 3), v(B, 4))} &= x_{u, (v(B, 4), v(B, 5))} + x_{u, (v(B, 4), v^{\text{dep}}(B, 4))} \\ x_{u, (v(B, 4), v(B, 5))} &= x_{u, (v(B, 2), v^{\text{dep}}(B, 5))} \\ x_{u, (v(B, 4), v^{\text{dep}}(B, 4))} &= x_{u, (v^{\text{dep}}(B, 4), v^{\text{arr}}(C, 5))} \\ x_{u, (v^{\text{dep}}(B, 4), v^{\text{arr}}(C, 5))} &= x_{u, (v^{\text{arr}}(C, 5), v(C, 5))} \\ x_{u, (v^{\text{dep}}(A, 1), v^{\text{arr}}(B, 2))} &= x_{u, (v^{\text{arr}}(B, 2), v(B, 2))} \\ x_{u, (v^{\text{arr}}(B, 2), v(B, 2))} &= x_{u, (v(B, 2), v(B, 3))}. \end{aligned}$$

and (2) additional constraints:

$$\begin{aligned} x_{u, (v(A, 1), v^{\text{dep}}(A, 1))} &= x_{u, (v^{\text{dep}}(B, 4), v^{\text{arr}}(C, 5))} \\ x_{u, (v(A, 2), v^{\text{dep}}(A, 2))} &= x_{u, (v^{\text{dep}}(B, 5), v^{\text{arr}}(C, 6))}. \end{aligned}$$

These constraints ensure that the path flows allocated on the departing edge, as per (2b), result in unique edge flows on the entire network.

## B Proof of Theoretical Results

### B.1 Proof of Proposition 3.3

Before presenting the proof, let us recall some important mathematical definitions and results which are crucial for the proof. First, we recall the definition of upper semicontinuous and lower semicontinuous correspondences.

**Definition B.1.** *A correspondence  $f : X \rightrightarrows Y$  is upper semicontinuous if for every sequence  $x_n \in X$  (with limit  $x$ ) and the sequence  $y_n \in f(x_n)$  which has a limit, then there exists  $y \in f(x)$  such that  $y = \lim_n y_n$ .*

**Definition B.2.** A correspondence  $f : X \rightrightarrows Y$  is lower semicontinuous if for every sequence  $x_n \in X$  (with limit  $x$ ) and  $y \in f(x)$ , then there exists a convergent sequence  $y_n \in f(x_n)$  with limit  $y$ .

Next, we recall the Kakutani fixed point theorem.

**Theorem B.3** (Kakutani Fixed Point Theorem). Suppose  $X$  is a non-empty, convex, and compact subset of  $\mathbb{R}^n$  and  $f : X \rightrightarrows X$  is a non-empty, compact-valued, convex-valued, and upper semicontinuous correspondence. Then  $f$  has a fixed point.

Finally, we recall Berge's maximum theorem.

**Theorem B.4** (Berge's Maximum Theorem). Consider the optimization problem  $\max_{x \in A(\theta)} F(x, \theta)$ . Let  $X(\theta)$  be the set of solutions of the preceding problem. If  $F$  is continuous in  $(x, \theta)$  and  $\theta \rightrightarrows A(\theta)$  is a non-empty, compact-valued, and continuous correspondence, then  $X(\theta)$  is a non-empty, compact-valued, and upper semicontinuous correspondence.

*Proof of Proposition 3.3.* The proof builds on a result about the existence of a competitive equilibrium in Fisher markets with auxiliary inequality constraints (Jalota et al., 2023). Particularly, our proof accounts for auxiliary *equality* constraints (resulting due to (2b)-(2c)).

In this result, we consider a relaxation of (2), by converting the integrality constraint to the positivity constraint. Consider the relaxed individual optimization problem of every agent stated below:

$$\max_{\bar{\mathbf{x}}_u} f_u(\bar{\mathbf{x}}_u) \tag{12a}$$

$$\text{s.t. } \mathbf{p}^\top \mathbf{x}_u + p_o x_{u,o} = w_u \tag{12b}$$

$$\tilde{\mathbf{a}}_u^\top \mathbf{x}_u + x_{u,\emptyset} = 1 \tag{12c}$$

$$\tilde{\mathbf{A}}_u \mathbf{x}_u = \mathbf{0} \tag{12d}$$

$$x_{u,o} \geq 0, x_{u,\emptyset} \geq 0, x_{u,e} \geq 0 \quad \forall e \in \tilde{\mathcal{E}}. \tag{12e}$$

To prove the existence result, we scale the problem such that the total budget of all agents is 1 and the capacity of each good is 1. To do this, for every  $e \in \tilde{\mathcal{E}}, u \in U$ , we scale any allocation  $x_{u,e}$  to  $x_{u,e}/\ell_e$ , scale  $\tilde{\mathbf{a}}_{u,e}$  to  $\tilde{\mathbf{a}}_{u,e} \cdot \ell_e$ , scale  $\tilde{\mathbf{A}}_u[:, e]$  to  $\tilde{\mathbf{A}}_u[:, e] \cdot \ell_e$ ,  $p_e$  to  $p_e \ell_e / W$ , and  $w_u$  to  $w_u / W$ , where  $W = \sum_u w_u$ . Note that under this change the solution of (12) does not change. Furthermore, due to the condition that  $v_{u,o} \geq 0$  and the variable  $x_{u,o}$  does not enter in the constraint (12c)-(12d), it is ensured that the budget constraint (12b) hold with equality.

Define  $\Delta_{|\tilde{\mathcal{E}}|} = \{\mathbf{p} \in \mathbb{R}^{|\tilde{\mathcal{E}}|} : \sum_{e \in \tilde{\mathcal{E}}} p_e = 1, p_e \geq 0 \forall e \in \tilde{\mathcal{E}}\}$ . Moreover, for every UAV  $u$ , define  $Y_u = \{\bar{\mathbf{x}}_u \in \mathbb{R}_{\geq 0}^{|\tilde{\mathcal{E}}|+2} : \tilde{\mathbf{a}}_u^\top \mathbf{x}_u + x_{u,\emptyset} = 1, \tilde{\mathbf{A}}_u \mathbf{x}_u = \mathbf{0}\}$ , and  $Q_u = \{\bar{\mathbf{x}}_u \in \mathbb{R}_{\geq 0}^{|\tilde{\mathcal{E}}|+2} : x_{u,r} \leq \Omega, \quad \forall r \in \tilde{\mathcal{E}} \cup \{o, \emptyset\}\}$  for some  $\Omega > 1$ . Define  $X = \prod_{u \in U} Q_u$ .

Define  $B_u(\mathbf{p}) = \{\bar{\mathbf{x}}_u \in Y_u : \mathbf{p}^\top \mathbf{x}_u + p_o x_{u,o} = w_u\}$ . Note that this set is non-empty, so we can always choose  $x_{u,\emptyset}$  to ensure that  $\mathbf{x}_u = \mathbf{0}$  and spend all the budget in the outside option  $o$ . Define

$$\tilde{\mathbf{x}}_u(\mathbf{p}) = \arg \max_{\bar{\mathbf{x}}_u \in Q_u \cap B_u(\mathbf{p})} f_u(\bar{\mathbf{x}}_u), \tag{13}$$

$$\tilde{\mathbf{p}}(\mathbf{x}) = \arg \max_{\mathbf{p} \in \Delta_{|\tilde{\mathcal{E}}|}} \mathbf{p}^\top \left( \sum_{u \in U} \mathbf{x}_u - \mathbf{1} \right). \tag{14}$$

Using the above definitions, define a correspondence  $h(\mathbf{x}, \mathbf{p}) = ((\tilde{\mathbf{x}}_u(\mathbf{p}))_{u \in U}, \tilde{\mathbf{p}}(\mathbf{x}))$ . We shall show that a fixed point of this mapping exists and is a fractional competitive equilibrium.

**Existence of a Fixed Point** We show that  $h$  satisfies the condition of the Kakutani fixed point theorem (cf. Theorem B.3), which ensures the existence of a fixed point. First, note that the domain of  $h$ , i.e.  $X \times \Delta_{|\tilde{\mathcal{E}}|}$ , is non-empty, compact and convex.

Next, we show that  $h$  is a non-empty, compact-valued, convex-valued, and upper semicontinuous correspondence. It is enough to show that  $\tilde{\mathbf{x}}_u(\mathbf{p})$  and  $\tilde{\mathbf{p}}(\mathbf{x})$  are non-empty, convex-valued and upper semicontinuous correspondences.

From (14), we observe that  $\tilde{\mathbf{p}}(\mathbf{x})$  is non-empty and convex-valued and is an optimal solution to a linear program with a non-empty, convex, and compact feasible set. All conditions for Berge's maximum theorem (cf. Theorem B.4) are satisfied, and therefore  $\tilde{\mathbf{p}}(\mathbf{x})$  is also compact-valued and upper semicontinuous.

Next, we show that  $\tilde{\mathbf{x}}_u(\mathbf{p})$  is non-empty and convex-valued as it is the optimizer of a linear function on a non-empty, convex, and compact set. Next, we leverage Theorem B.4 to show that this map is compact-valued and upper semicontinuous. First, we need to show that the correspondence  $g_u : \mathbf{p} \rightrightarrows Q_u \cap B_u(\mathbf{p})$  is a compact-valued and continuous correspondence. Compactness follows by construction, so the only thing remaining to show is continuity. To show continuity, it is enough to show that the mapping is upper semicontinuous and lower semicontinuous.

To show  $g_u$  is upper semicontinuous, consider a sequence  $(\bar{\mathbf{x}}_u^n, \mathbf{p}^n)$  such that  $\bar{\mathbf{x}}_u^n \in Q_u \cap B_u(\mathbf{p}^n)$ , which has limit  $(\bar{\mathbf{x}}_u, \mathbf{p})$ . Then, it is sufficient to establish that  $\bar{\mathbf{x}}_u \in Q_u \cap B_u(\mathbf{p})$ . Note that  $Q_u$  is compact, so if  $\bar{\mathbf{x}}_u^n \in Q_u$ , for every  $n \in \mathbb{N}$ , it follows that  $\bar{\mathbf{x}}_u \in Q_u$ . Furthermore, since  $\bar{\mathbf{x}}_u^n \geq 0$ , for every  $n \in \mathbb{N}$ , it follows that  $\bar{\mathbf{x}}_u \geq 0$ . Additionally, for every  $n \in \mathbb{N}$ ,  $\tilde{\mathbf{a}}_u^\top \bar{\mathbf{x}}_u^n + x_{u,\emptyset}^n = 1$ ,  $\tilde{\mathbf{A}}_u \bar{\mathbf{x}}_u^n = \mathbf{0}$ , it follows that  $\tilde{\mathbf{a}}_u^\top \bar{\mathbf{x}}_u + x_{u,\emptyset} = 1$ ,  $\tilde{\mathbf{A}}_u \bar{\mathbf{x}}_u = \mathbf{0}$ . Moreover, the continuity of product ensures that  $\mathbf{p}^{n\top} \bar{\mathbf{x}}_u^n + p_\circ x_{u,\circ}^n = w_u$ , for every  $n \in \mathbb{N}$ , implies  $\mathbf{p}^\top \bar{\mathbf{x}}_u + p_\circ x_{u,\circ} = w_u$ . This ensures that  $g_u$  is upper semicontinuous.

Next, we show that  $g_u$  is lower semicontinuous. To show this, it is sufficient to show that for any sequence  $\mathbf{p}^n$  with limit  $\mathbf{p}$  and any point  $\bar{\mathbf{x}}_u \in Q_u \times B_u(\mathbf{p})$  there is a sequence  $\bar{\mathbf{x}}_u^n \in Q_u \cap B_u(\mathbf{p}^n)$  such that  $\lim_{n \rightarrow \infty} \bar{\mathbf{x}}_u^n = \bar{\mathbf{x}}_u$ . Towards this goal, for every  $u \in U, e \in \tilde{\mathcal{E}}$ , we define  $\bar{\mathbf{x}}_u^n$  such that

$$x_{u,e}^n = \min \left\{ 1, \frac{w_u}{\mathbf{p}^{n\top} \mathbf{x}_u + p_\circ x_{u,\circ}} \right\} x_{u,e}, \quad x_{u,\emptyset}^n = 1 - \tilde{\mathbf{a}}_u^\top \mathbf{x}_u^n, \quad x_{u,\circ}^n = \frac{1}{p_\circ} (w_u - \mathbf{p}^{n\top} \mathbf{x}_u^n).$$

It is easy to check that  $\lim_{n \rightarrow \infty} \bar{\mathbf{x}}_u^n = \bar{\mathbf{x}}_u$ . The only thing remaining to show is that  $\bar{\mathbf{x}}_u^n \in Q_u \cap B_u(\mathbf{p}^n)$ . First, note that  $\tilde{\mathbf{a}}_u^\top \bar{\mathbf{x}}_u^n + x_{u,\emptyset}^n = 1$  follows by construction. Next, we show that  $x_{u,\emptyset}^n \geq 0$ . This is because

$$\begin{aligned} \tilde{\mathbf{a}}_u^\top \bar{\mathbf{x}}_u^n &= \min \left\{ 1, \frac{w_u}{\mathbf{p}^{n\top} \mathbf{x}_u + p_\circ x_{u,\circ}} \right\} \tilde{\mathbf{a}}_u^\top \mathbf{x}_u \leq \tilde{\mathbf{a}}_u^\top \mathbf{x}_u = 1 - x_{u,\emptyset} \\ \implies x_{u,\emptyset}^n &= 1 - \tilde{\mathbf{a}}_u^\top \bar{\mathbf{x}}_u^n \geq x_{u,\emptyset} \geq 0, \end{aligned}$$

where the inequality follows as  $\tilde{a}_{u,e} \geq 0, x_{u,e}^n \geq 0$ . Similarly, one can show that  $\tilde{\mathbf{A}}_u \bar{\mathbf{x}}_u^n = \mathbf{0}$ . Next, we note that budget constraints are satisfied by the construction of  $x_{u,\circ}^n$ . Finally, we show that  $x_{u,\circ}^n \geq 0$ . Indeed,

$$\mathbf{p}^{n\top} \bar{\mathbf{x}}_u^n = \min \left\{ 1, \frac{w_u}{\mathbf{p}^{n\top} \mathbf{x}_u + p_\circ x_{u,\circ}} \right\} \mathbf{p}^{n\top} \mathbf{x}_u \leq w_u.$$

Thus, we conclude that  $g_u$  is a compact-valued continuous correspondence. Thus, from Theorem B.3, we conclude that there exists  $(\bar{\mathbf{x}}^*, \mathbf{p}^*)$  such that  $\bar{\mathbf{x}}_u^* = \tilde{\mathbf{x}}_u(\mathbf{p}^*)$ ,  $\mathbf{p}^* = \tilde{\mathbf{p}}(\bar{\mathbf{x}}^*)$ ,  $\forall u \in U$ .

**Existence of a Fractional Competitive Equilibrium** We show that any fixed point corresponds to a fractional competitive equilibrium. First, using (13), we conclude that  $\bar{\mathbf{x}}_u^*$  is an optimal solution to (12). Second, note that  $\mathbf{p}^* \in \mathbb{R}_{\geq 0}^{|\tilde{\mathcal{E}}|}$  by construction. Next, we show that the capacity constraints are satisfied. We show this by contradiction. Suppose there exists an edge  $e' \in \tilde{\mathcal{E}}$  such that  $\sum_{u \in U} x_{u,e'}^* > 1$ . Then by (14), it must hold that

$$\sum_{e \in \tilde{\mathcal{E}}} p_e^* \left( \sum_{u \in U} x_{u,e}^* - 1 \right) \geq \sum_{e \in \tilde{\mathcal{E}}} p_e \left( \sum_{u \in U} x_{u,e}^* - 1 \right), \quad \forall \mathbf{p} \in \Delta_{|\tilde{\mathcal{E}}|}.$$

We claim that  $\sum_{e \in \tilde{\mathcal{E}}} p_e^* (\sum_{u \in U} x_{u,e}^* - 1) = 0$ . Indeed,

$$\sum_{e \in \tilde{\mathcal{E}}} p_e^* (\sum_{u \in U} x_{u,e}^* - 1) = \sum_{u \in U} \sum_{e \in \tilde{\mathcal{E}}} p_e^* x_{e,u}^* - \sum_{e \in \tilde{\mathcal{E}}} p_e^* = \sum_{u \in U} w_u - 1 = 0.$$

Thus, we conclude that

$$0 \geq \sum_{e \in \tilde{\mathcal{E}}} p_e \left( \sum_{u \in U} x_{u,e}^* - 1 \right), \quad \forall \mathbf{p} \in \Delta_{|\tilde{\mathcal{E}}|}. \quad (15)$$

Since  $\sum_{u \in U} x_{u,e'}^* > 1$ , we can select  $p_{e'} = 1$  and 0 otherwise, which would violate the above inequality, a contradiction.

Next, we show that if  $p_e^* > 0$  then  $\sum_{u \in U} x_{u,e}^* = 1$ . This follows immediately from the fact that capacity constraints are satisfied and the fact that  $\sum_{e \in \tilde{\mathcal{E}}} p_e^* (\sum_{u \in U} x_{u,e}^* - 1) = 0$ . This completes the proof.  $\square$

## B.2 Proof of Proposition 3.5

Observe that for any fixed value of  $\omega \in \mathbb{R}^{|U|}$ , the optimization problem (3) is a convex optimization problem. Define the Lagrangian as follows.

$$\begin{aligned} \mathcal{L}_{\mathbf{P}} = & \sum_{u \in U} (w_u + \omega_u) \log(f_u(\bar{\mathbf{x}}_u)) - \sum_{u \in U} p_{\circ} x_{u,\circ} - \mathbf{p}^\top \left( \sum_{u \in U} \mathbf{x}_u - \ell \right) \\ & - \sum_{u \in U} \lambda_u (\tilde{\mathbf{a}}_u^\top \mathbf{x}_u + x_{u,\emptyset} - 1) - \sum_{u \in U} \kappa_u^\top \tilde{\mathbf{A}}_u \mathbf{x}_u + \sum_{u \in U} \mu_u^\top \bar{\mathbf{x}}_u, \end{aligned}$$

where  $\mathbf{p} \in \mathbb{R}_{\geq 0}^{|\tilde{\mathcal{E}}|}$  is the Lagrange multiplier corresponding to constraint (3b),  $\lambda = (\lambda_u)_{u \in U} \in \mathbb{R}^{|U|}$  is the Lagrange multiplier corresponding to (3c),  $\kappa = (\kappa_u)_{u \in U} \in \mathbb{R}^{K|U|}$  is the Lagrange multiplier corresponding to (3d), and  $\mu = (\mu_u)_{u \in U} \in \mathbb{R}_{\geq 0}^{|\tilde{\mathcal{E}}|}$  is the Lagrange multiplier corresponding to (3e).

We observe that, for a given  $\omega$ , any optimal solution  $\bar{\mathbf{x}}^\dagger$  of (3) with optimal dual multipliers  $(\mathbf{p}^\dagger, \lambda^\dagger, \kappa^\dagger, \mu^\dagger)$

will satisfy the following first order conditions of optimality.

$$0 \geq \begin{cases} \frac{(w_u + \omega_u)}{f_u(\bar{\mathbf{x}}_u^\dagger)} v_{u,e} - p_e^\dagger - \tilde{a}_{u,e} \lambda_u^\dagger - (\tilde{\mathbf{A}}_u^\top \tilde{\kappa}_u^\dagger)_e & \text{if } e \in \tilde{\mathcal{E}} \\ \frac{(w_u + \omega_u)}{f_u(\bar{\mathbf{x}}_u^\dagger)} v_{u,\circ} - p_\circ & \text{if } e = \circ \\ \frac{(w_u + \omega_u)}{f_u(\bar{\mathbf{x}}_u^\dagger)} v_{u,\emptyset} - \lambda_u^\dagger & \text{if } e = \emptyset. \end{cases} \quad (16)$$

Furthermore, the complementary slackness conditions are given by

$$0 = \begin{cases} \frac{(w_u + \omega_u)}{f_u(\bar{\mathbf{x}}_u^\dagger)} v_{u,e} x_{u,e}^\dagger - p_e^\dagger x_{u,e}^\dagger - \tilde{a}_{u,e} x_{u,e}^\dagger \lambda_u^\dagger - (\tilde{\mathbf{A}}_u^\top \tilde{\kappa}_u^\dagger)_e x_{u,e}^\dagger & \text{if } e \in \tilde{\mathcal{E}} \\ \frac{(w_u + \omega_u)}{f_u(\bar{\mathbf{x}}_u^\dagger)} v_{u,\circ} x_{u,\circ}^\dagger - p_\circ^\dagger x_{u,\circ}^\dagger & \text{if } e = \circ, \quad p_e^\dagger \left( \sum_{u \in U} x_{u,e}^\dagger - \ell_e \right) = 0, \quad \forall e \in \tilde{\mathcal{E}}. \\ \frac{(w_u + \omega_u)}{f_u(\bar{\mathbf{x}}_u^\dagger)} v_{u,\emptyset} x_{u,\emptyset}^\dagger - \lambda_u x_{u,\emptyset}^\dagger & \text{if } e = \emptyset \end{cases} \quad (17)$$

Similarly, the Lagrangian of the (relaxed) individual optimization problem (12) is given by

$$\mathcal{L}_I = f_u(\bar{\mathbf{x}}_u) - \tilde{\omega}_u (\mathbf{p}^\top \mathbf{x}_u + p_\circ x_{u,\circ} - w_u) - \tilde{\lambda}_u (\tilde{\mathbf{a}}_u^\top \mathbf{x}_u + x_{u,\emptyset} - 1) - \sum_{u \in U} \tilde{\kappa}_u^\top \tilde{\mathbf{A}}_u \mathbf{x}_u + \tilde{\mu}_u^\top \bar{\mathbf{x}}_u,$$

where  $\tilde{\omega}_u \in \mathbb{R}$  is the Lagrange multiplier corresponding to the budget constraint,  $\tilde{\lambda}_u \in \mathbb{R}$  is the Lagrange multiplier corresponding to (12c),  $\tilde{\kappa}_u \in \mathbb{R}^K$  is the Lagrange multiplier corresponding to (12d), and  $\tilde{\mu}_u \in \mathbb{R}_{\geq 0}^{|\tilde{\mathcal{E}}|}$  is the Lagrange multiplier corresponding to the positivity constraint (12e).

We observe that, for a given  $\mathbf{p}$ , any optimal solution  $\bar{\mathbf{x}}^\dagger$  of (12) with optimal dual multipliers  $(\tilde{\omega}^\dagger, \tilde{\lambda}^\dagger, \tilde{\kappa}^\dagger, \tilde{\mu}^\dagger)$  satisfies the following first order conditions of optimality.

$$0 \geq \begin{cases} v_{u,e} - \tilde{\omega}_u^\dagger p_e - \tilde{\lambda}_u^\dagger \tilde{a}_{u,e} - (\tilde{\mathbf{A}}_u^\top \tilde{\kappa}_u^\dagger)_e & \text{if } e \in \tilde{\mathcal{E}} \\ v_{u,\circ} - \tilde{\omega}_u^\dagger p_\circ & \text{if } e = \circ \\ v_{u,\emptyset} - \tilde{\lambda}_u^\dagger & \text{if } e = \emptyset. \end{cases} \quad (18)$$

Furthermore, using the complementary slackness condition, we obtain

$$0 = \begin{cases} v_{u,e} x_{u,e}^\dagger - \tilde{\omega}_u^\dagger p_e x_{u,e}^\dagger - \tilde{\lambda}_u^\dagger \tilde{a}_{u,e} x_{u,e}^\dagger - (\tilde{\mathbf{A}}_u^\top \tilde{\kappa}_u^\dagger)_e x_{u,e}^\dagger & \text{if } e \in \tilde{\mathcal{E}} \\ v_{u,\circ} x_{u,\circ}^\dagger - \tilde{\omega}_u^\dagger p_\circ x_{u,\circ}^\dagger & \text{if } e = \circ \\ v_{u,\emptyset} x_{u,\emptyset}^\dagger - \tilde{\lambda}_u^\dagger x_{u,\emptyset}^\dagger & \text{if } e = \emptyset. \end{cases} \quad (19)$$

In order to prove Proposition 3.5, we show that if there exists  $\omega^*$  such that  $\omega^* = \lambda^\dagger(\omega^*)$  then  $(\bar{\mathbf{x}}^\dagger(\omega^*), \mathbf{p}^\dagger(\omega^*))$  is a fractional-competitive equilibrium. It is sufficient to verify the following:

- (i) By fixing the prices to  $\mathbf{p}^\dagger(\omega^*)$ ,  $\bar{\mathbf{x}}_u^\dagger(\omega^*)$  is an optimal solution of (12), for every  $u \in U$ ;
- (ii) the capacity constraints are satisfied at every resource;
- (iii)  $p_e^\dagger(\omega^*) \geq 0$  for every  $e \in \tilde{\mathcal{E}}$ ; and
- (iv) if  $p_e^\dagger(\omega^*) > 0$  for some  $e \in \tilde{\mathcal{E}}$ , then  $\sum_{u \in U} x_{u,e}^\dagger(\omega^*) = \ell_e$ .

It is immediate to note that (ii) – (iv) are satisfied due to dual and primal feasibility conditions of (3). It only remains to show (i).

To show (i), it is sufficient to show that there exists  $\tilde{\omega}_u^\dagger, \tilde{\lambda}_u^\dagger, \tilde{\kappa}_u^\dagger$  such that  $(\bar{\mathbf{x}}_u^\dagger(\omega^*), \tilde{\omega}_u^\dagger, \tilde{\lambda}_u^\dagger, \tilde{\kappa}_u^\dagger)$  satisfies the conditions (18)-(19), and the budget constraint in (12b) holds.

Setting the optimal Lagrange variable of (3b) with  $\omega_u = \lambda_u$  then the optimal solution  $x^*$  of (3) is the solution of individual optimization problem for all players with price  $\mathbf{p}^*$ .

By primal optimality conditions in (16), we obtain

$$0 \geq \begin{cases} v_{u,e} - \frac{f_u(\bar{\mathbf{x}}_u^\dagger)}{(w_u + \omega_u^*)} p_e^\dagger - \frac{f_u(\bar{\mathbf{x}}_u^\dagger)}{(w_u + \omega_u^*)} \tilde{a}_{u,e} \lambda_u^\dagger - \frac{f_u(\bar{\mathbf{x}}_u^\dagger)}{(w_u + \omega_u^*)} (\tilde{\mathbf{A}}_u^\top \tilde{\kappa}_u^\dagger)_e & \text{if } e \in \tilde{\mathcal{E}} \\ v_{u,\circ} - \frac{f_u(\bar{\mathbf{x}}_u^\dagger)}{(w_u + \omega_u^*)} p_\circ & \text{if } e = \circ \\ v_{u,\emptyset} - \frac{f_u(\bar{\mathbf{x}}_u^\dagger)}{(w_u + \omega_u^*)} \lambda_u^\dagger & \text{if } e = \emptyset. \end{cases} \quad (20)$$

The preceding equation is equivalent to the primal optimality condition of individual optimization problem in (18) if we select  $\tilde{\lambda}_u^\dagger = \frac{f_u(\bar{\mathbf{x}}_u^\dagger)}{(w_u + \omega_u^*)} \lambda_u^\dagger$ ,  $\tilde{\omega}_u = \frac{f_u(\bar{\mathbf{x}}_u^\dagger)}{(w_u + \omega_u^*)}$  and  $\tilde{\kappa}_u^\dagger = \frac{f_u(\bar{\mathbf{x}}_u^\dagger)}{(w_u + \omega_u^*)} \kappa_u^\dagger$ . Similarly, (19) is also satisfied with the same choice. Finally, we show that individual budget constraint (12b) holds. For this we use the complementary slackness condition in (17) by summing all three cases in (17). For every  $u \in U$ , we obtain

$$0 = \frac{(w_u + \omega_u^*)}{f_u(\bar{\mathbf{x}}_u^\dagger)} f_u(\bar{\mathbf{x}}_u^\dagger) - \mathbf{p}^{\dagger\top} \mathbf{x}_u^\dagger - p_\circ x_{u,\circ}^\dagger - \lambda_u^\dagger (\tilde{\mathbf{a}}_u^\top \mathbf{x}_u^\dagger + x_{u,\emptyset}^\dagger) - \kappa_u^{\dagger\top} \tilde{\mathbf{A}}_u^\top \mathbf{x}_u^\dagger.$$

Consequently, using (3c)-(3d) we obtain

$$\begin{aligned} 0 &= (w_u + \omega_u^*) - \mathbf{p}^{\dagger\top} \mathbf{x}_u^\dagger - p_\circ x_{u,\circ}^\dagger - \lambda_u^\dagger \\ &= w_u - \mathbf{p}^{\dagger\top} \mathbf{x}_u^\dagger - p_\circ x_{u,\circ}^\dagger, \end{aligned}$$

where in the last equation we used the fact that  $\omega^* = \lambda^\dagger$ . This completes the proof.

## C Table of Notations

Notation	Description
$\mathcal{G}$	Graph representing the airspace
$\tilde{\mathcal{G}}$	Graph representing the time-extended airspace
$\mathcal{R}$	Set of regions/sectors in the urban airspace
$\tilde{\mathcal{E}}$	Set of edges indicating feasible movement between contiguous regions
$C^{\text{arr}}(r, t), C^{\text{dep}}(r, t), C^{\text{stay}}(r, t)$	Maximum number of vehicles that can arrive, depart, or stay in the region $r \in R$ at time $t$
$W$	Auction window time interval
$U(t)$	Set of AAM vehicles arriving in the system at time $t$
$M_u$	Menu of time-trajectories (air corridors) for AAM vehicle $u$
$R_u$	Set of routes in the menu of AAM vehicle $u$
$\nu(r, t)$	Node in region $r$ and time $t$
$v_{u,s}$	Valuation (utility) of vehicle $u$ for path $s$
$p_o, p_e$	Price of the outside edge option, price of an edge $e \in \tilde{\mathcal{E}}$
$x_{u,e}$	Allocation of an AAM vehicle $u$ to edge $e$
$x_{u,o}$	Allocation of an AAM vehicle $u$ to outside option
$\mathbf{x}_u$	The vector $(x_{u,e})_{e \in \tilde{\mathcal{E}}}$
$\bar{\mathbf{x}}_u$	The vector $[\mathbf{x}_u^\top, x_{u,o}, x_{u,\emptyset}]^\top$
$w_u$	Budget of AAM vehicle $u$ (air credits)
$e^*(s)$	Departing edge from the origin region on the route $s$
$\ell_e$	Supply of edge $e \in \tilde{\mathcal{E}}$
$\bar{\mathbf{x}}_u$	Optimal solution for the IOP with optimal price $\mathbf{p}^*$
$f_u(\bar{\mathbf{x}}_u)$	Total utility of allocation $\bar{\mathbf{x}}_u$
$\tilde{\mathcal{E}}^{(1)}, \tilde{\mathcal{E}}^{(2)}, \tilde{\mathcal{E}}^{(3)}, \tilde{\mathcal{E}}^{(4)}$	Arrival (landing), departing (take-off), stay (parking), and transit (air-corridor) edges